J Stat Phys (2008) 130: 343–371
DOI 10.1007/s10955-007-9427-5

Evolution of the Probability Measure for the Majda Model: New Invariant Measures and Breathing PDFs

Roberto Camassa · Zhi Lin · Richard M. McLaughlin

Received: 27 December 2006 / Accepted: 7 September 2007 / Published online: 9 October 2007

Abstract In 1993, Majda proposed a simple, random shear model from which scalar intermittency was rigorously predicted for the invariant probability measure of passive tracers. In this work, we present an integral formulation for the tracer measure, which leads to a new, comprehensive study on its temporal evolution based on Monte Carlo simulation and direct numerical integration. An interesting, non-monotonic "breathing" phenomenon is discovered from these results and carefully defined, with a solid example for special initial data to predict such phenomenon. The signature of this phenomenon may persist at long time, characterized by the approach of the PDF core to its infinite time, invariant value. We find that this approach may be strongly dependent on the non-dimensional Péclet number, of which the invariant measure itself is independent. Further, the "breathing" PDF is recovered as a new invariant measure in a distinguished time scale in the diffusionless limit. Rigorous asymptotic analysis is also performed to identify the Gaussian core of the invariant measures, and the critical rate at which the heavy, stretched exponential regime propagates towards the tail as a function of time is calculated.

Keywords Turbulent transport · Scalar intermittency · Invariant measures

1 Introduction

An important class of problems concerns understanding how complicated fluid flows mix and distribute numerous scalar quantities. Examples include the distribution of ozone in the stratosphere, salt and carbon in the oceans, and vapor in the troposphere, and these distributions ultimately play an important role in understanding the dynamics of the atmospheres and oceans. Detailed measurements of these distributions often depict time series which admit stochastic properties in both the flow fields, as well as in the transported quantities themselves [1, 13, 20, 26, 27]. These observations have led to an effort to understand these

R. Camassa · Z. Lin (✉) · R.M. McLaughlin
Department of Mathematics, University of North Carolina, CB#3250 Phillips Hall, 27599-3250 Chapel Hill, NC, USA
e-mail: zlin@email.unc.edu

observations in partial differential equations with random coefficients [9–12, 15, 20, 21, 23–25]. The simplest of these equations is a diffusing passive scalar equation with a prescribed random, incompressible advection. Such dynamics are linear, but involve random coefficients, and the fundamental question is to predict the probability measure which the scalar quantity inherits from the random advection. The linearity of the evolution makes such problems tractable, but nonetheless extremely difficult and it is often necessary to appeal to Monte Carlo simulation to gain insight. There are extremely few mathematical analyses on which to base the validity of such simulations. For fluid flows which are random shear layers, several important mathematical results have been obtained, either for cases in which the scalar is fluctuating in the presence of a large scale, mean gradient [5], or in the freely decaying scalar case [6–8, 16–19, 28]. We focus upon the freely decaying case in this article.

Batchelor [3] and later Kraichnan [15] introduced a class of rapidly fluctuating, Gaussian random, linear flows. Kraichnan observed that in the white noise limit, closed evolution equations are available for the scalar mean and covariance, and later it has been recognized that closed evolution equations for arbitrary statistical moments of the scalar field are available in this limit [18]. Passive scalars diffusing in the presence of such flows have received much attention, particularly in attempting to calculate the tail behavior of the scalar single point PDF, either in the freely decay case or in the pumped (randomly sourced) case [2, 6, 8, 10–12, 16, 19, 28]. Typically, instanton-type methods have been applied to attempt to compute this tail behavior, which has been shown to follow stretched exponential distributions. Beyond this tail information, little more is known regarding the complete evolving scalar probability measure, and many open problems exist.

Majda introduced a model in 1993 [16] through which the Nth statistical moment of the tracer may be expressed as an explicit N-dimensional integral. This model assumes that the velocity field has a simple spatial structure which is a linear shear layer multiplied by a Gaussian white noise process. Such a flow may be recognized as a sum of a particular Kraichnan model and a random rotation, but it is distinct from Batchelor and Kraichnan flows. Nonetheless, complete, rigorous mathematical results are available for such a random shear problem which successfully predict stretched exponential tail distributions.

Bronski and McLaughlin rigorously computed the large N asymptotics of these integrals in 2000 [7, 8], which yielded the probability density function (PDF) tail of this measure. The tail falls off as a stretched exponential, with a simple formula for the stretching exponent set by the correlation length of the random initial data for the tracer, which is assumed to be a Gaussian random field. Subsequently, a large deviation theory for this problem was developed by Vanden-Eijnden [28] which extended these results to linear shears multiplied by fractional Brownian motion. For the case of a decaying passive scalar, this is the most complete calculation of the PDF, and essentially all predictions have either been in the form of moments, or in studies of the tail of the distribution.

Here, we present new, dynamical behavior for the PDF which occurs within this model using a combination of simulation and rigorous analysis. For random initial data whose two-point spatial correlation possesses multiple peaks, we document that the PDF admits an interesting "breathing" phenomenon. This non-monotonic behavior is characterized by an initial growth of the probability density in the core beyond those set by the long time, limiting invariant measure. Simultaneously, the concavity of the PDF is anomalously larger than the invariant measure over several standard deviations. Subsequently, the PDF core in turn decays to the invariant measure. Alternatively, for initial data not possessing a multiply-peaked correlation function, the evolution to the invariant measure is monotonic in the core, and the concavity in the core region is lower than the invariant measure. This behavior we

first observed in Monte Carlo simulations is carefully documented through a more accurate numerical evaluation of an integral representation of the PDF we present. In turn, we identify a new invariant measure which captures this breathing behavior through a distinguished, diffusionless limit. Lastly, for a special class of multiply-peaked correlation functions, we rigorously predict this breathing phenomenon. Additionally, we establish that the invariant measure always has a Gaussian core for a wide range of initial cut-off functions, and compute the explicit time scales for the PDF tail to approach the invariant measure.

The paper is organized as follows. In Sect. 2, we overview the main results. In Sect. 3, we review the Majda Model and in Sect. 4 we present the integral representations for the complete PDF. In Sect. 5, we document and define the breathing phenomenon using Monte Carlo simulations and present highly accurate verification using direct numerical evaluation of the integral formula. Then we show rigorously that the PDF core is always larger than the initial Gaussian, and that the signature of breathing may persist at long time. In Sect. 6 we present the asymptotic analysis for the integral formula which shows that the PDF core is Gaussian for the invariant measure. Additionally, a unique scaling between long time and small diffusion is calculated and shown to give a new invariant measure which possesses all the breathing features as observed in the simulations. Further, the rate of convergence to the invariant measure in the tail is explicitly calculated in this section. In Sect. 7, a rigorous analytical prediction of the breathing phenomenon is presented for a special class of initial data. Lastly, in the Appendix, we give all details regarding the asymptotic and direct numerical PDF evaluation of the L^2 norm of Brownian motion which is central to this work.

2 Main Results

In this paper, we propose the following:

1. The integral representation for the renormalized tracer PDF of the Majda shear model is established via the Law of Total Probability. This representation enables the usage of numerical integration to study the spatio-temporal evolution of the tracer PDF, whose results are verified by Monte Carlo simulations, but with much improved computation cost and accuracy.
2. From the numerical results for the PDF evolution, a *non-monotonic*, transitional phenomenon is discovered and then defined as "breathing". An explicit example is proposed in Sect. 7 to rigorously predict such phenomenon.
3. The signature of breathing phenomenon, namely the PDF core exceeding its infinite time invariant limit, may persist at long time, depending critically on the local concavity of the cut-off function near $k = 0$. Specifically, for cut-offs possessing a local expansion $1 + Ak^\gamma, k \to 0^+, \gamma \in (0, 1)$, the PDF core approaches the invariant measure from above if and only if $A > 0$. When $\gamma > 1$, the persistence is also strong dependent on the non-dimensional Péclet number and detailed discussion and example are presented. Moreover, the PDF core is rigorously proven to be larger than or equal to its initial Gaussian value $(2\pi)^{-1/2}$ at all positive times.
4. Rigorous asymptotic analysis shows that for a broad class of initial cut-off functions, the long time invariant PDF has a Gaussian core (locally quadratic). In other words, the stretched exponential behavior of the tails does not extend to the core.
5. Through the integral representation of the tracer PDF in the integral form, the "breathing" PDF is identified as the consequence of choosing specific cut-off functions, by exploring different time scalings in the diffusionless limit.

6. As an extension to previous work, the critical rate at which the stretched exponential region in the tracer PDF propagates towards the tail is identified, by following the curves $\bar{T} = Ct^{\gamma}$ in the tracer ($\bar{T}$)-time (t) phase plane.

3 Problem Formulation

Consider the Majda Model [16] for a passive tracer governed by the non-dimensional, *random advection-diffusion equation* with planar initial condition:

$$T_t + \gamma(t)xT_y = \frac{1}{\mathrm{Pe}}\Delta_{x,y}T, \quad T(x, y, t = 0) = T_0(y), \tag{3.1}$$

where Pe is the Péclet number which characterizes the importance of molecular diffusion and $\gamma(t)$ is the temporal white noise satisfying

$$\langle \gamma(t) \rangle_{\gamma} = 0, \qquad \langle \gamma(t)\gamma(t') \rangle_{\gamma} = \delta(t - t') \tag{3.2}$$

and $T_0(y)$ is a Gaussian Random Field with the spectral representation

$$T_0(y) = \int_{-\infty}^{\infty} e^{2\pi iky}|k|^{\alpha/2}\hat{\phi}_0(k)dW(k). \tag{3.3}$$

Here the function $\hat{\phi}_0(k)$ is a rapidly decreasing cut-off function satisfying $\hat{\phi}_0(k) = \hat{\phi}_0(-k)$ and $\hat{\phi}_0(0) \neq 0$. Traditionally $\hat{\phi}_0(k)$ is renormalized so that $\hat{\phi}_0(0) = 1$. However, as we will see in (4.4), this is not necessary and therefore we do not renormalize it. The spectral parameter α determines the spatial correlation scales of the initial scalar field, with increasing α corresponding to shorter range correlation. Lastly, $dW(k)$ is a complex white noise with

$$\langle dW(k) \rangle_W = 0, \qquad \langle dW(k)dW(k') \rangle_W = \delta(k + k')dk\, dk'. \tag{3.4}$$

Given a fixed realization of $\gamma(t)$, $t > 0$, (3.1) can be solved (in the Stratonovich's sense) [28] for all times as

$$T(x, y, t) = \int_{-\infty}^{\infty} e^{2\pi ik[y - B(t)x]}|k|^{\alpha/2}\hat{\phi}_0(k)e^{-\frac{4\pi^2k^2}{\mathrm{Pe}}[t+\xi(t)]}dW(k), \tag{3.5}$$

where $B(t) = \int_0^t \gamma(s)ds$ is a Wiener Process and $\xi(t) = \int_0^t B^2(s)ds$ is the L^2-norm of the Wiener Process. It is known that a soluble, closed form moment equation for the N-point correlation function $\langle \prod_{i=1}^{N} T(x_i, y_i, t) \rangle_{W,\gamma}$ is available for this problem [16, 19]. Furthermore, this random process $\xi(t)$ can be transformed into a random variable η, utilizing the rescaling property of the Wiener process [28], namely,

$$\xi(t) = t^2\eta = t^2 \int_0^1 B^2(s)ds, \quad \text{in law.} \tag{3.6}$$

Therefore, we can replace $\xi(t)$ by $t^2\eta$ to simplify the calculations while the statistical properties of the tracer field remain the same.

It's easy to check via cluster expansion that the moment of arbitrary order of T defined in (3.5) is independent of x and y [16, 19]. Thus this is a homogeneous random field at all

times. Without loss of generality, for single-point statistics, it suffices to study the statistics of

$$T(0,0,t)=\int_{-\infty}^{\infty}|k|^{\alpha/2}\hat{\phi}_0(k)e^{-\frac{4\pi^2k^2}{\mathrm{Pe}}[t+t^2\eta]}dW(k). \tag{3.7}$$

Notice that in this solution for T, the randomness that the tracer inherited from the random shear is manifested through a single random variable, η, as the previous work [6, 28] has recovered. Next we will see how the full tracer PDF is connected to the PDF of η. It has been established [7, 8, 28] that for finite Pe the invariant (infinite time) probability measure of the renormalized tracer, denoted as $\bar{T}$, has stretched exponential tails controlled by the parameter α:

$$P_{\bar{T}}(\bar{T})\sim A(\alpha)e^{-B(\alpha)|\bar{T}|^{\frac{4}{3+\alpha}}+o(|\bar{T}|^{\frac{4}{3+\alpha}})},\quad |\bar{T}|\to\infty. \tag{3.8}$$

4 The Law of Total Probability

Given any fixed realization of $\gamma(t)$ for $t\geq 0$, or equivalently in law, η, (3.5) suggests that T is still a Gaussian Random Field *conditionally*, with conditional PDF

$$P_{T|\eta}(T|\eta)=\frac{1}{\sqrt{2\pi\sigma_c^2(\eta,t)}}e^{-\frac{T^2}{2\sigma_c^2(\eta,t)}} \tag{4.1}$$

in which the conditional variance $\sigma_c^2(\eta,t)$ can be computed from (3.7) as

$$\sigma_c^2(\eta,t)=\langle T^2\rangle_W=\int_{-\infty}^{\infty}|k|^{\alpha}\hat{\phi}_0^2(k)e^{-\frac{8\pi^2k^2}{\mathrm{Pe}}(t+t^2\eta)}dk. \tag{4.2}$$

Further, if we renormalize T with its unconditional variance [16]

$$\sigma_{uc}^2(t)=\langle T^2\rangle_{W,\eta}=\int_{-\infty}^{\infty}\frac{|k|^{\alpha}\hat{\phi}_0^2(k)e^{-\frac{8\pi^2k^2t}{\mathrm{Pe}}}}{\sqrt{\cosh\frac{4\pi kt}{\sqrt{\mathrm{Pe}}}}}dk, \tag{4.3}$$

so that $\bar{T}=\frac{T}{\sigma_{uc}(t)}$ has unit variance, very similar formula for $P_{\bar{T}|\eta}(\bar{T}|\eta)$ follows with σ_c^2 in (4.1) replaced by

$$\sigma^2(\eta,t)=\frac{\sigma_c^2(\eta,t)}{\sigma_{uc}^2(t)}. \tag{4.4}$$

Then *the Law of Total Probability* implies that the unconditional PDF for $\bar{T}(0,0,t)$, which we denote simply as $\bar{T}$ from now on since it is a homogeneous field in space, can be calculated as

$$P_{\bar{T}}(\bar{T})=\int_0^{\infty}P_{\bar{T}|\eta}(\bar{T}|\eta)P_{\eta}(\eta)d\eta. \tag{4.5}$$

From this formulation, we can see that the time evolution of the tracer PDF is completely manifested in the time dependence of σ^2. Finally, $P_{\eta}(\eta)$ is known to have the inverse Laplace Transform representation [6, 28]:

$$P_{\eta}(\eta)=\frac{1}{2\pi i}\int_{-i\infty}^{i\infty}\prod_{k=1}^{\infty}\left(1+\frac{2s}{(k-\frac{1}{2})^2\pi^2}\right)^{-\frac{1}{2}}e^{s\eta}ds, \tag{4.6}$$

and the detailed derivation will be presented in the Appendix.

5 Full PDF Dynamics: Monte Carlo Simulation and Numerical Integration

Previous work has explored the long time, tail behavior of the renormalized tracer PDF, $P_{\bar{T}}(\bar{T})$, and has rigorously predicted the emergence of heavy-tailed distributions. However, its finite time and the finite tracer value dynamics remains an open question. In this section, we use two different numerical approaches to simulate the evolution of the PDF. These two sets of results support the validity of the simulation algorithms by their mutual agreement, and further illuminate the analytical study discussed in Sect. 6. In particular, a nontrivial, transitional phenomenon which was not documented before is revealed by the numerical results.

5.1 Monte Carlo Simulation for the Tracer PDF

As a universal, powerful tool for stochastic problems, Monte Carlo simulation can be readily developed in light of the random solution (3.5) for the Majda model, to illustrate the temporal evolution of the renormalized tracer PDF, $P_{\bar{T}}(\bar{T})$, where $\bar{T} = \frac{T}{\sigma_{uc}(t)}$ and σ_{uc} is defined in (4.3) so that $\langle \bar{T}^2 \rangle_{W,\eta} = 1$. In particular, the Fourier integral is first truncated for $|k| > K$ (K fixed) and then is discretized with $2N_k$ Fourier modes as

$$T(x,y,t) \approx \sum_{j=-N_k}^{N_k-1} e^{\frac{2\pi i j K}{N_k}[y-B(t)x]-\frac{4\pi^2 j^2 K^2}{N_k^2 \mathrm{Pe}}[t+\xi(t)]} \left|\frac{jK}{N_k}\right|^{\frac{\alpha}{2}} \hat{\phi}_0\left(\frac{jK}{N_k}\right)(w_j^r + i w_j^i), \tag{5.1}$$

where w_j^r, w_j^i are the real and imaginary parts of the discretized complex white noise $dW(k)$, respectively and thus they are i.i.d. Gaussian random numbers with variance $\frac{K}{N_k}$. With a simple random number generator, the summing in (5.1) for one realization of the random field $T(x,y,t)$ can be made highly efficient via FFT (Fast Fourier Transform) given a realization of $\gamma(t), t \geq 0$ and (w_j^r, w_j^i), $j = -N_k, \ldots, N_k - 1$. Furthermore, at each time step, a histogram of $\bar{T}$ as an approximation to $P_{\bar{T}}(\bar{T})$ requires a sample of $R_f \times R_\gamma$ realizations of $T(0,0,t)$ computed by (5.1) and renormalized by the sample variance, where R_f is the number of realizations of the initial field, (w_j^r, w_j^i) and R_γ is the number of realizations of the random shear, $(B(t), \xi(t))$.

To obtain the realizations for the Wiener process $B(t)$ and its L^2-norm, $\xi(t)$, we utilize the scaling properties of $B(t)$ and $\xi(t)$, namely, $B(t) = \sqrt{t}B(1)$ and $\xi(t) = t^2\eta$ *in law*, with η defined in (3.6). Moreover, the Law of Large Numbers guarantees that as the temporal discretization, N_t, goes to infinity, the following approximations converge with probability 1:

$$B(1) \approx \sum_{j=1}^{N_t} dB_j \quad \text{and} \quad \eta \approx \frac{1}{N_t}\sum_{l=1}^{N_t}\left(\sum_{j=1}^{l} dB_j\right)^2, \tag{5.2}$$

where dB_j, $j = 1, 2, \ldots, N_t$ are i.i.d., Gaussian random variables with variance $\frac{1}{N_t}$. Consequently, instead of generating realizations for $(B(t), \xi(t))$ at each time step, we can repeatedly use the same sample of $(B(1), \eta)$ at different times and multiply it with proper time scalings and thus the temporal complexity of the simulation is greatly reduced.

To summarize, the total computation count of the Monte Carlo simulation consists of the one-time generation of the samples for (w_j^r, w_j^i), $j = -N_k, \ldots, N_k - 1$ and $(B(1), \eta)$, which

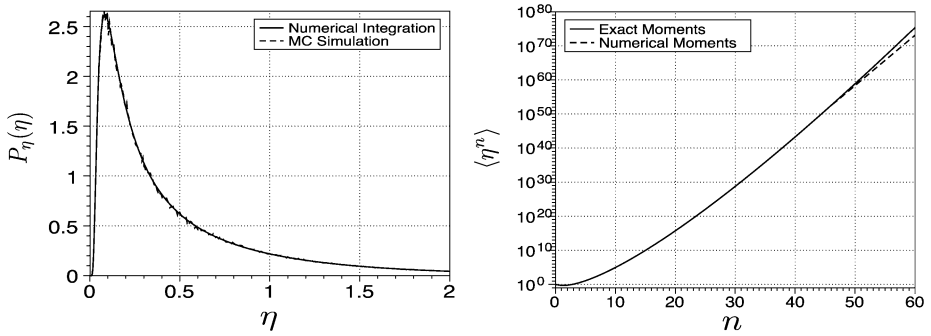

Fig. 1 The statistics of η. *Left*: numerical approximations for $P_\eta(\eta)$. *Right*: the accuracy of numerical moments

are of order $R_f N_k$ and $R_\gamma N_t$ respectively, and summing (5.1) with FFT at each time step, which is of order $R_f R_\gamma N_k \ln N_k$. It is obvious that other than the influences of discretizations N_k and N_t, the computation complexity is greatly intensified when performing the FFT summing, by the fact that both of the two sources of randomness, the initial random field and the random shear, need enough realizations to obtain good approximations to the statistical distributions, namely, the product $R_f R_\gamma$ is large. In our simulations, by setting $N_k = N_t = 512$ and $R_f = R_\gamma = 10^6$, we obtain reasonably smooth, statistically stationary histograms that agree with the PDF numerically computed as described in Sect. 5.2.

5.2 Numerical Integration for the Tracer PDF

Although the Monte Carlo simulations are straightforward to implement, we need some independent methodology to verify the above results. And more importantly, robust as Monte Carlo simulations are, the statistical convergence is generally slow, which in this problem leads to intense computation complexity as mentioned before. Alternatively, utilizing the integral forms which we discussed in Sect. 4, we can directly compute the tracer PDF in its simple integral form (4.5) with numerical quadratures, to avoid the complex simulation. However, with only the integral representations (4.2), (4.3) and (4.6) for σ_c^2, σ_{uc}^2 and $P_\eta(\eta)$, respectively, we also have to evaluate them numerically. In particular, the evaluation of $P_\eta(\eta)$ will be discussed in Appendix, where we find the analytic continuation of $(\cosh\sqrt{2s})^{-1/2}$ along the integration path, the imaginary axis, or transform the original Bromwich integral (4.6) into a series of real integrals via (9.6). Moreover, for very small or very large values of η, $P_\eta(\eta)$ can be asymptotically approximated by (9.5) and (9.7).

Figure 1 shows the results evaluating the integrator, compared with the Monte Carlo simulated PDF generated by setting $N_t = 10^3$ and $R_\gamma = 10^6$ as discussed in Sect. 5.1. In the right panel, the accuracy of numerically integrated $P_\eta(\eta)$ is estimated by comparing the numerical moments with the exact moments utilizing

$$\langle \eta^n \rangle = (-1)^n n! \frac{\partial^n}{\partial s^n} \frac{1}{\sqrt{\cosh\sqrt{2s}}}\bigg|_{s=0} \approx \Delta\eta \sum_{i=1}^{10^6} (i\Delta\eta)^n \tilde{P}_\eta(i\Delta\eta), \tag{5.3}$$

where $\Delta\eta = 10^{-4}$ and $\tilde{P}_\eta$ is the numerically integrated PDF for η.

Furthermore, the robustness of the integrator has also been verified by the numerical convergence test in which the relative error decreases with increasing number of points used in the quadrature.

5.3 Numerical Results

Applying the methods discussed above, we obtain two sets of numerical results from Monte Carlo simulation and numerical integration, which agree with each other, as shown in Fig. 2. Here we set $\hat{\phi}_0(k) = e^{-k^2/70}$ and $1/\mathrm{Pe} = 10^{-5}$, and implemented the numerical approximations for three different values of α, each at three different times. We observe the gradual transition of the renormalized tracer PDF from its initial state, unit Gaussian, to its long time limiting state, stretched exponential (3.8). In fact, for this combination of $\hat{\phi}_0$ and Pe, the PDFs remains almost identical after $t = 1000$.

From Fig. 2, it seems that the stretched exponential region in each of the invariant measures extends to the core, $\bar{T} = 0$, at large times. However, the PDF in fact remains Gaussian (locally quadratic) in the small interval $|\bar{T}| \ll 1$ if we zoom in into these intervals, and we will analyze this in Sect. 6. Also, since the PDF tails are observed to be heavier than Gaussian, this suggests that there are also regions "lighter" than Gaussian, namely, for some intermediate values of $|\bar{T}|$, $P_{\bar{T}}(\bar{T})$ has to be less than its initial Gaussian value, $\exp(-\frac{\bar{T}^2}{2})/\sqrt{2\pi}$, from the conservation of probability, $\int_{-\infty}^{\infty} P_{\bar{T}}(\bar{T}) \equiv 1$. For example, this property is clearly true for the family of stretched exponential distribution with exponents between $(0, 2)$.

5.4 Observation: The "Breathing" PDF

As expected, the above numerical results verify that the renormalized PDF becomes stationary at sufficient large times and the shape is controlled by the value of the parameter α, while the effect of the initial cut-off function $\hat{\phi}_0$ vanishes. In particular, the long time invariant measure for fixed α and Pe, which will be derived in Sect. 6, reads

$$P_{\bar{T}}(\bar{T}) \to \frac{\sqrt{C(\alpha)}}{\sqrt{2\pi}} \int_0^{\infty} \eta^{\frac{\alpha+1}{4}} e^{-\frac{\bar{T}^2}{2} C(\alpha) \eta^{\frac{\alpha+1}{2}}} P_\eta(\eta) d\eta, \quad t \to \infty, \tag{5.4}$$

where $C(\alpha)$ is a function of α alone and it will be defined later in this section. However, there is a striking difference between the PDF evolutions for different initial cut-off functions $\hat{\phi}_0$, which is shown in Fig. 3, where the numerically integrated PDFs are plotted.

In particular, at each intermediate time, the probability measure for $\hat{\phi}_0(k) = \exp(-\frac{k^2}{70})$ is just an "interpolation" between the initial unit Gaussian and the long time invariant measure (5.4), which is asymptotically equal to $Ae^{-B|\bar{T}|+o(|\bar{T}|)}$ in the tails when $\alpha = 1$ and thus is approximately straight lines as plotted in the panels for $t = 1000$. In a sharp contrast, when $\hat{\phi}_0(k) = \exp(-\frac{(|k|-20)^2}{70})$, at $t = 50$, there exist large intervals of $\bar{T}$ on which the evolving probability density is significantly larger than the invariant measure. However, we also know that at any finite time, the PDF has Gaussian tails which will be "lighter" than the invariant exponential tails. Therefore, the anomalous behavior we observe in Fig. 3 for $\hat{\phi}_0(k) = \exp(-\frac{(|k|-20)^2}{70})$ cannot be recovered from tail asymptotics that have been done for this model. Essentially, what really distinguishes the two cases in Fig. 3 is that for some values of $|\bar{T}|$, the tracer PDF inherited from $\hat{\phi}_0(k) = \exp(-\frac{(|k|-20)^2}{70})$ has a larger *concavity* than that of the corresponding invariant measure. As another example to illustrate this difference, now consider two different initial cut-off functions whose induced PDFs at three different times are compared in Fig. 4, where the thick, solid line always corresponds to the intermediate transitional PDF of interest. Clearly, the same discrepancy as shown in Fig. 3 emerges: for $\hat{\phi}_0(k) = \frac{1}{100+k^{10}}$, the concavity of the intermediate measure at $t = 50$ does not exceed

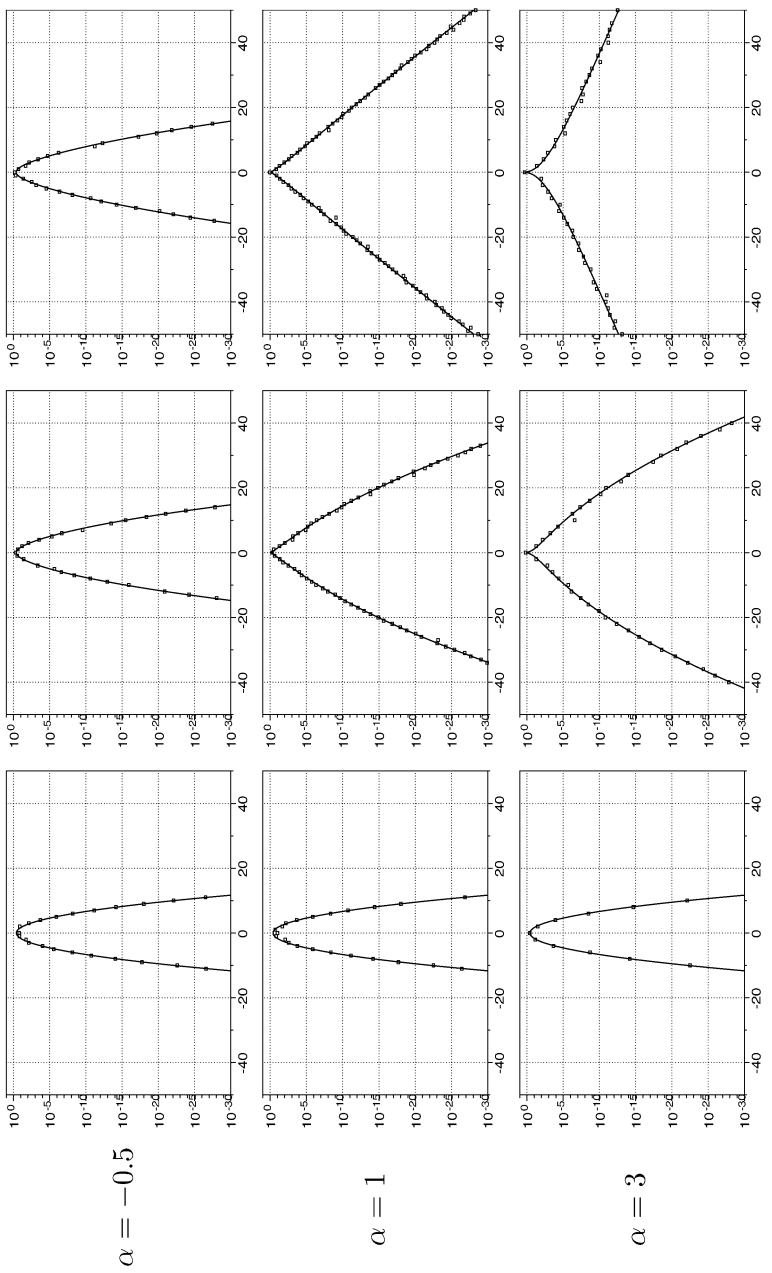

Fig. 2 PDF evolutions when $\hat{\phi}_0(k) = e^{-\frac{k^2}{70}}$ and $\mathrm{Pe} = 10^5$ obtained by Monte Carlo simulation (□), and numerical integration (–). *Horizontal axis*: renormalized tracer $\bar{T}$. *Vertical axis*: probability density $P_{\bar{T}}(\bar{T})$

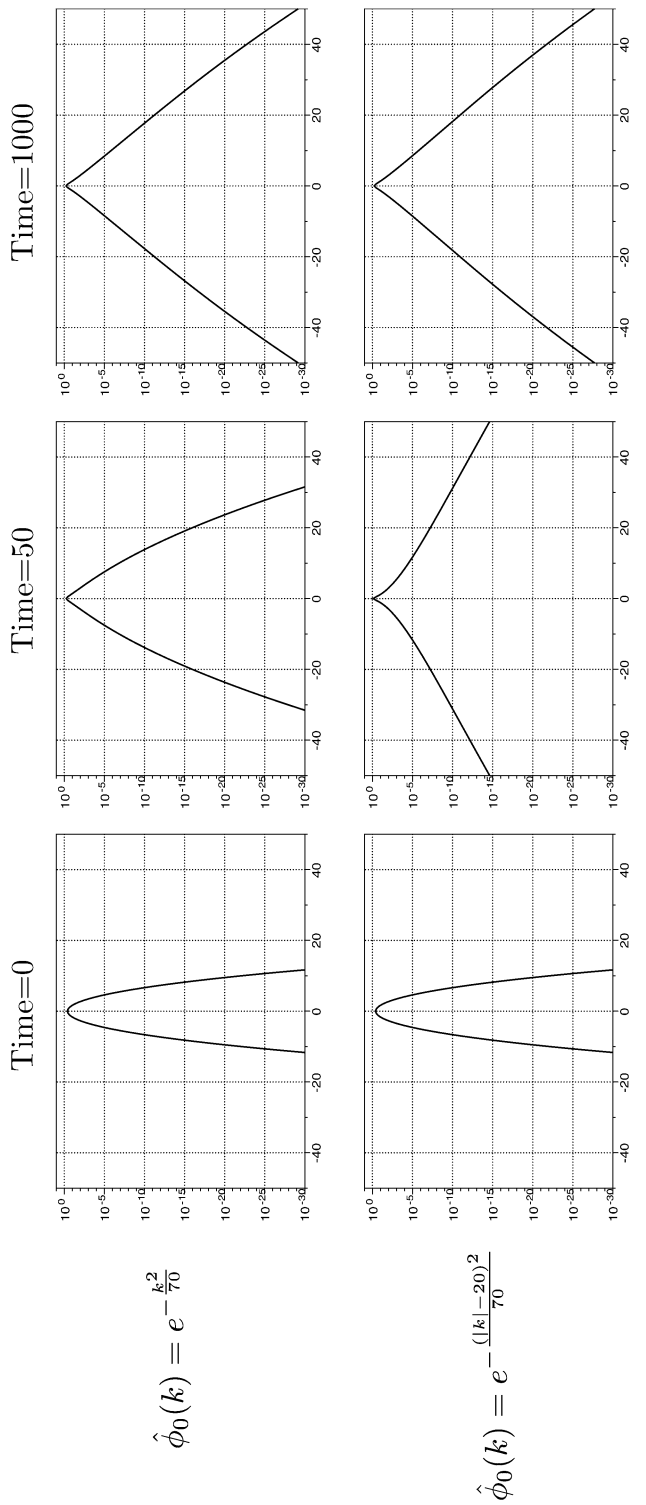

Fig. 3 PDF evolutions for different $\hat{\phi}_0(k)$, where $\alpha = 1$, $\mathrm{Pe} = 10^5$

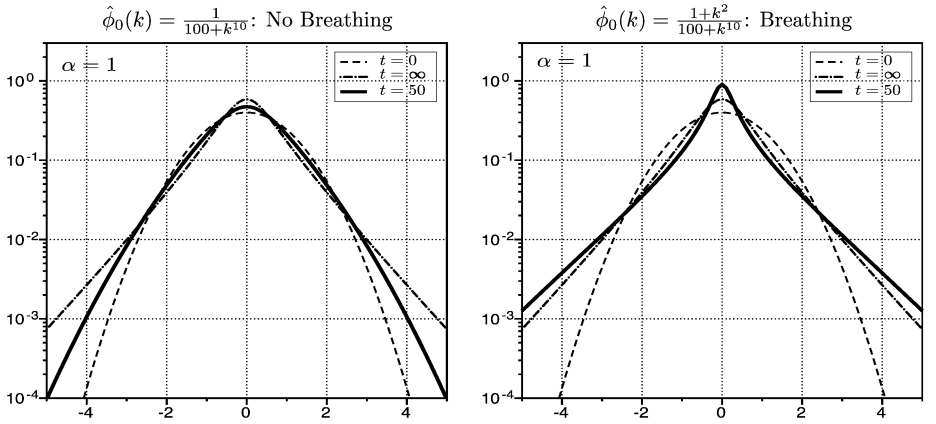

Fig. 4 PDF evolutions for different $\hat{\phi}_0(k)$, where $\alpha = 1$, $\mathrm{Pe} = 10^5$. *Horizontal axis*: renormalized tracer $\bar{T}$. *Vertical axis*: probability density $P_{\bar{T}}(\bar{T})$

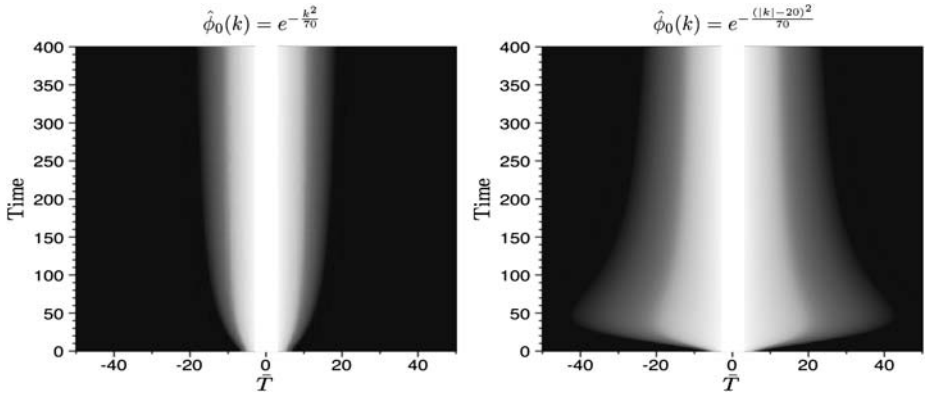

Fig. 5 Logarithm of PDF evolutions for different $\hat{\phi}_0(k)$, where $\alpha = 1$, $\mathrm{Pe} = 10^5$

that of the invariant measure anywhere; while for $\hat{\phi}_0(k) = \frac{1+k^2}{100+k^{10}}$ and for $|\bar{T}|$ approximately between 0 and 3, the intermediate measure has a larger concavity than the invariant measure.

Figure 5 further illustrates the dynamical evolution of the PDFs from $t = 0$ to $t = 400$, where the logarithm, $\ln P_{\bar{T}}(\bar{T})$, is plotted in grayscale with a uniform ramp between $[-50, 1]$. Here $\ln P_{\bar{T}}(\bar{T})$ has larger values in bright regions whereas it is smaller in dark regions. Again, the difference between the PDFs at intermediate times is evident from left to right.

There is another intriguing phenomenon that co-exists with the concavity anomaly discussed above, which can be observed in Fig. 4. This can also been seen in the analogous figure for $\hat{\phi}_0(k) = \exp(-\frac{k^2}{70})$ and $\hat{\phi}_0(k) = \exp(-(|k| - 20)^2/70)$. In the right panel, $P_{\bar{T}}(0; t = 50)$ is larger than both $P_{\bar{T}}(0; t = 0)$ and $P_{\bar{T}}(0; t = \infty)$, which implies that $P_{\bar{T}}(0)$ has to evolve *non-monotonically* in time, whereas in the left panel such non-monoticity cannot be seen and $P_{\bar{T}}(0; t = 0) < P_{\bar{T}}(0; t = 50) < P_{\bar{T}}(0; t = \infty)$. In fact, when $\hat{\phi}_0(k) = \frac{1}{100+k^{10}}$, $P_{\bar{T}}(\bar{T})$ varies monotonically in time from its initial value at $t = 0$, to its invariant value at $t = \infty$ for most fixed values of $\bar{T}$. However, in the case, where $\hat{\phi}_0(k) = \frac{1+k^2}{100+k^{10}}$,

these evolutions are not monotonic, as shown in Fig. 6, where $P_{\bar{T}}(\bar{T})$ is computed at $t = n\Delta t,\ n = 0, 1, \ldots, 50$ and $\Delta t = 25$.

Although the same non-monotonic evolution can also be recovered for the case where $\hat{\phi}_0(k) = \frac{1}{100+k^{10}}$ for $\bar{T}$ in some small intervals away from 0, the discrepancy in the temporal dynamics of $P_{\bar{T}}(0)$ does distinguishes these two cases. Therefore, to identify this special *"breathing"* phenomenon, we propose the following definition based on the temporal monotonicity of $P_{\bar{T}}(0)$:

Definition For any fixed $\varepsilon > 0$, the renormalized tracer PDF $P_{\bar{T}}(\bar{T})$ is said to *"breath"* in time if there exists at least one time $t = t^*, 0 < t^* < \infty$ such that $P_{\bar{T}}(\bar{T} = 0; t = t^*) > P_{\bar{T}}(\bar{T} = 0; t \to \infty)$, where the infinite time limit of the PDF core can be derived from (5.4) via

$$P_{\bar{T}}(\bar{T} = 0; t \to \infty) := P_\infty(0) = \sqrt{\frac{C(\alpha)}{2\pi}} \langle \eta^{\frac{\alpha+1}{4}} \rangle_\eta. \tag{5.5}$$

As we will see next, since the limit (5.5) is always larger than the initial Gaussian core, $1/\sqrt{2\pi}$, this definition also implies that the PDF core has at least one temporal maximum if the PDF breathes. To study the temporal evolution of the PDF core, first we have the following:

Proposition 1 (PDF core larger than Gaussian) *For any $t > 0$, the renormalized PDF core is larger than its initial Gaussian value, namely,*

$$P_{\bar{T}}(0) \geq \frac{1}{\sqrt{2\pi}}, \quad \forall t > 0. \tag{5.6}$$

Further, numerical results suggest that the inequality is in fact strict. To prove (5.6), we consider the special case of the Law of Total Probability (4.5), where $\bar{T} = 0$:

$$P_{\bar{T}}(0) = \frac{1}{\sqrt{2\pi}} \int_0^\infty \frac{1}{\sqrt{\sigma^2(\eta, t)}} P_\eta(\eta) d\eta = \frac{1}{\sqrt{2\pi}} \left\langle \frac{1}{\sqrt{\sigma^2(\eta, t)}} \right\rangle_\eta. \tag{5.7}$$

Then the proposition follows trivially by *Jensen's inequality* [22] and the definition of σ^2 in (4.4) since

$$\left\langle \frac{1}{\sqrt{\sigma^2(\eta, t)}} \right\rangle_\eta \geq \frac{1}{\sqrt{\langle \sigma^2(\eta, t) \rangle_\eta}} = 1. \tag{5.8}$$

Moreover, we find that the breathing phenomenon observed for bimodal cut-offs and defined above is more than a transient behavior, and may persist for all time. In particular, $P_{\bar{T}}(0)$ may approach its invariant limit from above or below at long time. We establish that the bimodality in the cut-off function is the critical signature for observing a PDF core exceeding its infinite time limit at large times:

Proposition 2 (Long time persistence of breathing) *Suppose that α, Pe are fixed and*

$$\hat{\phi}_0^2(k) \sim 1 + Ak^\gamma, \quad k \to 0^+, \tag{5.9}$$

with $A \neq 0$ and $\gamma > 0$, then whether the breathing persists at long time, namely, $P_{\bar{T}}(0) > P_\infty(0)$ for any t sufficiently large, is determined by the initial cut-off function $\hat{\phi}_0$. Specifically,

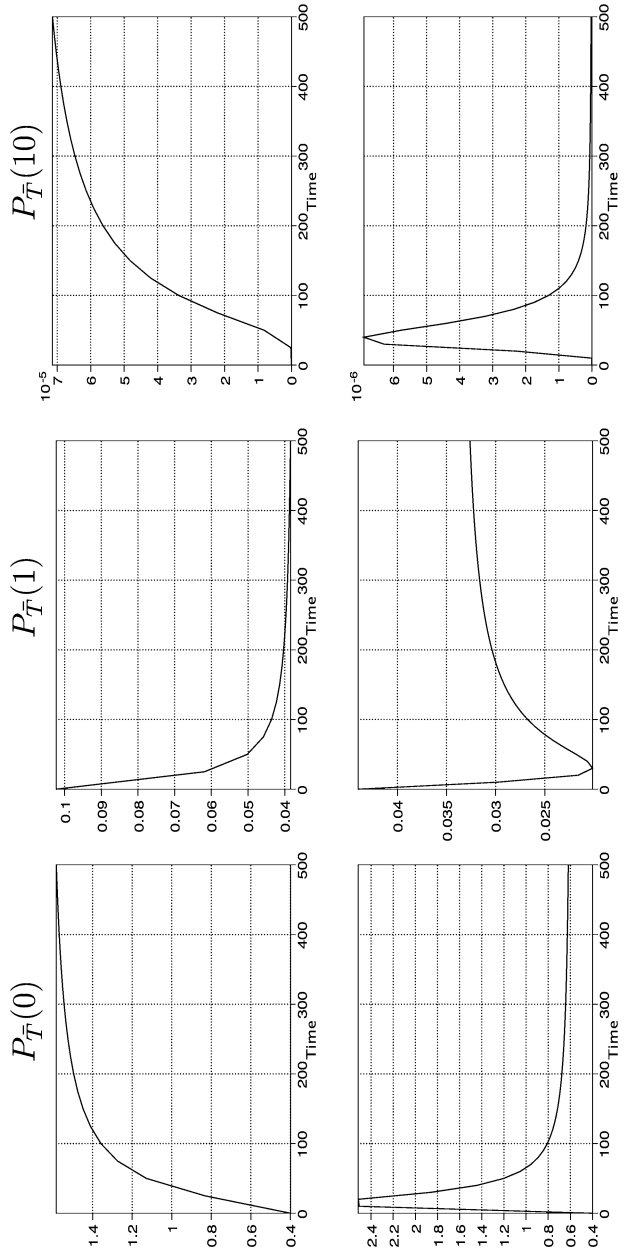

Fig. 6 Fixed-point PDF evolutions for different $\hat{\phi}_0(k)$, where $\alpha = 1$, $\mathrm{Pe} = 10^5$. *Horizontal axis*: time. *Vertical axis*: $P_{\bar{T}}(\bar{T})$ with $\bar{T}$ fixed

1. *For* $\gamma < 1$, *the breathing persists at long time* if and only if $A > 0$.
2. *For* $\gamma = 1$, *the breathing persists at long time* if and only if $A > d^*(\alpha, \mathrm{Pe})$ *where* d^* *is a critical value determined by* α *and* Pe.
3. *For* $\gamma > 1$, *the breathing does* not *persist at long time.*

Moreover, when breathing does not persist at long time, $P_{\bar{T}}(0) < P_\infty(0)$ *for any* t *sufficiently large.*

This proposition follows from two lemmas we present below, whose rigorous proofs are not the focus of this paper and thus they are not described in details here. First, we investigate the long time asymptotic property for the renormalized conditional variance defined in Sect. 4. Recall

$$\sigma^2(\eta, t) := \frac{\sigma_c^2(\eta, t)}{\sigma_{uc}^2(t)} = \frac{\int_{-\infty}^{\infty} |k|^\alpha \hat{\phi}_0^2(k) e^{-\frac{8\pi^2 k^2}{\mathrm{Pe}}(t+t^2\eta)} dk}{\int_{-\infty}^{\infty} \frac{|k|^\alpha \hat{\phi}_0^2(k) e^{-\frac{8\pi^2 k^2 t}{\mathrm{Pe}}}}{\sqrt{\cosh \frac{4\pi k t}{\sqrt{\mathrm{Pe}}}}} dk}. \tag{5.10}$$

Lemma 1 *Under the assumptions of Proposition 2, for any* $\varepsilon > 0$,

$$\begin{aligned}
\frac{1}{\sqrt{\sigma^2(\eta, t)}} &\sim \left(\frac{\frac{2^{\frac{\alpha+1}{2}}\Gamma(\frac{\alpha+1}{2})}{(\eta+1/t)^{\frac{\alpha+1}{2}}} + \frac{A(\mathrm{Pe})^{\gamma/2}}{t^\gamma} \frac{2^{\frac{\alpha+\gamma+1}{2}}\Gamma(\frac{\alpha+\gamma+1}{2})}{(4\pi)^\gamma (\eta+1/t)^{\frac{\alpha+\gamma+1}{2}}}}{2I(\alpha) - \frac{I(\alpha+2)}{t} + \frac{A(\mathrm{Pe})^{\gamma/2}}{t^\gamma} \frac{2I(\alpha+\gamma)}{(4\pi)^\gamma}} \right)^{-1/2} \\
&\sim \begin{cases} \sqrt{C(\alpha)}\, \eta^{\frac{\alpha+1}{4}} \left[1 + t^{-1} f(\alpha, \gamma, \eta) \right], & \gamma > 1, \\ \sqrt{C(\alpha)}\, \eta^{\frac{\alpha+1}{4}} \left[1 + t^{-1} \left(f(\alpha, 1, \eta) + A\sqrt{\mathrm{Pe}}\, g(\alpha, 1, \eta) \right) \right], & \gamma = 1, \\ \sqrt{C(\alpha)}\, \eta^{\frac{\alpha+1}{4}} \left[1 + t^{-\gamma} A(\mathrm{Pe})^{\gamma/2} g(\alpha, \gamma, \eta) \right], & \gamma < 1, \end{cases}
\end{aligned} \tag{5.11}$$

uniformly for any $\eta \in [\varepsilon, +\infty)$ *as* $t \to \infty$, *where*

$$\begin{aligned}
C(\alpha) &= \frac{2^{\frac{1-\alpha}{2}}}{\Gamma(\frac{\alpha+1}{2})} I(\alpha) = \frac{2^{\frac{1-\alpha}{2}}}{\Gamma(\frac{\alpha+1}{2})} \int_0^\infty \frac{u^\alpha du}{\sqrt{\cosh u}}, \\
f(\alpha, \gamma, \eta) &= \frac{\alpha+1}{4\eta} - \frac{I(\alpha+2)}{4I(\alpha)}, \\
g(\alpha, \gamma, \eta) &= \frac{1}{(4\pi)^\gamma} \left[\frac{I(\alpha+1)}{2I(\alpha)} - \frac{2^{\gamma/2}\Gamma(\frac{\alpha+\gamma+1}{2})}{2\eta^{\gamma/2}\Gamma(\frac{\alpha+1}{2})} \right].
\end{aligned} \tag{5.12}$$

In $\eta \in [0, \varepsilon)$, the asymptotic estimate (5.11) is valid only pointwise. But due to the super-exponential decay of $P_\eta(\eta)$ shown in the Appendix, excluding a small neighborhood near 0 from the integral (5.7) does not change the asymptotic expansion of $P_{\bar{T}}(0)$ at long times. The rigorous details to validate this exclusion are tedious and are not pursued in this paper. To prove the above lemma, one only needs to apply Watson's Lemma [4] to expand σ_c^2 in (5.10) by taking $(t + t^2\eta)$ to be the large parameter. For σ_{uc}^2, rescaling with $u = \frac{4\pi k t}{\sqrt{\mathrm{Pe}}}$, expanding the integrand and a term-by-term integration yield its asymptotic estimate in (5.11).

Comparing with (5.5), we can see that the leading order in the expansion (5.11) yields the infinite time limit of the PDF shown in (5.5). To further determine whether the PDF core

approaches the limiting value (5.5) from above or below, we substitute $(\sigma^2)^{-1/2}$ in (5.7) with its asymptotic expansion (5.11) and study the sign of the first order correction after integration. Consequently, Proposition 2 is the immediate corollary of the lemma presented below, which can be proven for special values $\alpha = 4m - 1, \gamma = 2m, m = 1, 2, \ldots$. For general α and γ, we verified numerically that the lemma also holds but the rigorous proof requires further study and is beyond the scope of this paper.

Lemma 2 *For any $\alpha > -1$ and $\gamma > 0$,*

$$F(\alpha,\gamma) := \int_0^\infty \eta^{\frac{\alpha+1}{4}} f(\alpha,\gamma,\eta) P_\eta(\eta) d\eta < 0 < G(\alpha,\gamma) := \int_0^\infty \eta^{\frac{\alpha+1}{4}} g(\alpha,\gamma,\eta) P_\eta(\eta) d\eta. \tag{5.13}$$

Lemma 1 and 2 show quantitatively how the long time persistence of breathing is determined by A, γ for fixed α and Pe, and in turn by the behavior of the cut-off function near $k = 0$. Moreover, we observe in (5.11) that A changes the core behavior only via the term $A(\mathrm{Pe})^{\gamma/2}$. For example, when $\gamma = 1$,

$$P_{\bar{T}}(0)|_t \sim P_\infty(0) + t^{-1}[F(\alpha,\gamma) + A\sqrt{\mathrm{Pe}}\, G(\alpha,\gamma)], \quad t \to \infty. \tag{5.14}$$

Then the breathing persists at long times if $A > d^*(\alpha, \mathrm{Pe}) := -F/(G\sqrt{\mathrm{Pe}}) > 0$. Notice that if $A > 0$, the cut-off function is automatically not uni-modal.

Consider the two bimodal cut-off functions for which we previously observed the short-time breathing phenomenon, when $\alpha = 1$ and $\mathrm{Pe} = 10^5$: For $\hat{\phi}_0(k) = \exp(-\frac{(|k|-20)^2}{70})$, we have $\gamma = 1$ and $A\sqrt{\mathrm{Pe}} = 8\sqrt{10^5}/7 > d^*(1) \approx 45$ and thus $P_{\bar{T}}(0) > P_\infty(0)$ at long times; in contrast, for $\hat{\phi}_0(k) = \frac{1+k^2}{100+k^{10}}$, $\gamma = 2 > 1$, and so $P_{\bar{T}}(0) < P_\infty(0)$ at long times, although the PDF core exceeds the invariant value at short times. This implies the existence of a critical time when the core takes a minimum for cut-off functions which induce short-time breathing, but make the core approach the invariant limit from below, namely, $\gamma > 1$. In such cases, the Péclet dependent terms in (5.11) are second order corrections, and consequently are washed away in sufficiently long time. To promote these terms to first order, one may consider a distinguished limit which links the Péclet number with time. This time scale is actually evident in the asymptotic expansion (5.11), namely, $t^* \propto (\mathrm{Pe})^{\frac{\gamma}{2(\gamma-1)}}$ since this scaling balances the terms $1/t$ and $(t/\sqrt{\mathrm{Pe}})^{-\gamma}$ and consequently, the latter is promoted into the first correction term. We verify this scaling numerically for $\alpha = 1$ and $\hat{\phi}_0(k) = \frac{1+k^2}{100+k^{10}}$ and $\gamma = 2$, by varying Pe and identifying the critical time, t^*, when $P_{\bar{T}}(0)$ takes a temporal minimum. The result is log–log plotted in Fig. 7 and the curve is very close to a straight line with the slope $\frac{\gamma}{2(\gamma-1)} = 1$, as predicted by the distinguished scaling.

One of the reasons that we are interested in this phenomenon is that the probability (the integral of the density) concentrates near $|\bar{T}| = 0$, which measures what values of the tracer are most likely to be observed. Therefore, its temporal evolution is important to our understanding of the random tracer field. It should be noted that when breathing occurs for $\hat{\phi}_0(k) = \frac{1+k^2}{100+k^{10}}$ or $\hat{\phi}_0(k) = \exp(-\frac{(|k|-20)^2}{70})$, the relationship between the concavity anomaly in the PDF and the temporal non-monotonicity of $P_{\bar{T}}(0)$ is an open question, and we adopt the above definition for breathing due to its simplicity and unambiguity. As it will be shown in Sects. 6 and 7, the occurrence of this non-monotonic transition, or "breathing," is not universal for general $\hat{\phi}_0$. From the specific choices of $\hat{\phi}_0$ that invoke "breathing" as shown in Figs. 3, 4, 5 and 6, it is natural to conjecture that the non-monotonicity in $\hat{\phi}_0$ itself

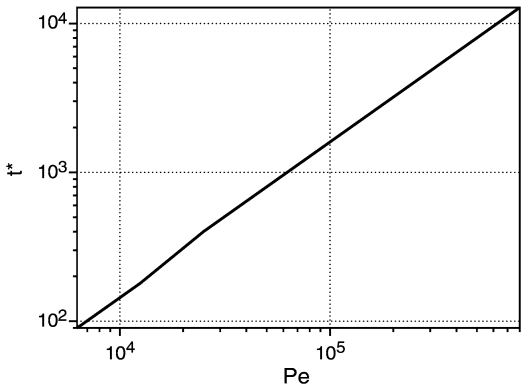

Fig. 7 The time-Péclet scaling for temporal minimum of $P_{\bar{T}}(0)$, when $\hat{\phi}_0(k) = \frac{1+k^2}{100+k^{10}}$

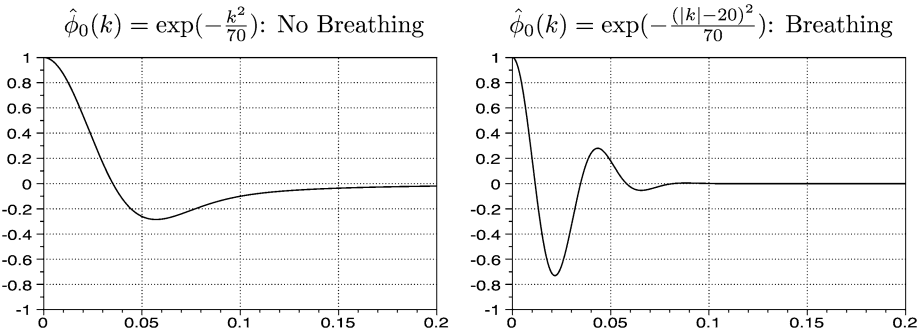

Fig. 8 Two-point correlation functions for different $\hat{\phi}_0(k)$, where $\alpha = 1$. *Horizontal axis*: r: distance between two points in space. *Vertical axis*: $R(r)$: two-point correlation of the initial random field

contributes. In particular, neither of the functions $\exp(-\frac{(|k|-20)^2}{70})$ and $\frac{1+k^2}{100+k^{10}}$ is monotonic in $|k|$, while $\exp(-\frac{k^2}{70})$ and $\frac{1}{100+k^{10}}$ are monotonic and no "breathing" is observed for these two cases. Moreover, the definition for breathing above can be extended to define "multiple breathing", when $P_{\bar{T}}(\bar{T}=0)$ has multiple temporal extrema $t_i^*, i = 1, 2, \ldots$. In fact, we have seen *double breathing*, where $P_{\bar{T}}(\bar{T}=0)$ has two temporal maxima, if we set $\hat{\phi}_0$ to be quad-modal, for example, in the form of $\exp(-\frac{(|k|-M_1)^2}{V_1}) + R\exp(-\frac{(|k|-M_2)^2}{V_2})$, for some values of M_1, M_2, V_1, V_2 and R. This further supports the conjecture that breathing is caused by the non-monotonicity of $\hat{\phi}_0$ and the number of temporal maxima in $P_{\bar{T}}(\bar{T}=0)$ is related to that of maxima in $\hat{\phi}_0(k)$ with respect to $|k|$. Figure 8 suggests that a fundamental difference can be observed between the ensuing two-point correlation functions for the initial data in the physical domain,

$$R(r) = \frac{\langle T_0(y)\, T_0(y+r)\rangle_W}{\sqrt{\langle T_0^2(y)\rangle_W \langle T_0^2(y+r)\rangle_W}} = \frac{\int_{-\infty}^{\infty} |k|^\alpha e^{2\pi i k r} \hat{\phi}_0^2(k) dk}{\int_{-\infty}^{\infty} |k|^\alpha \hat{\phi}_0^2(k) dk}. \tag{5.15}$$

As seen in this figure, there are multiple peaks in the correlation function for $\hat{\phi}_0(k) = \exp(-\frac{(|k|-20)^2}{70})$, while there is only one at $r = 0$ for $\hat{\phi}_0(k) = \exp(-\frac{k^2}{70})$.

We also investigated the evolution of the correlation $R(r)$ in time, however they do not seem to exhibit anything particularly intriguing. Therefore, the relationship between this

multiply-peaked behavior and the breathing PDF remains an open question which will be addressed in the future work. It should be noted that the breathing at short time which we observed in Figs. 3, 4, 5 and 6 is also related to the bimodality of the initial cutoff. However, the asymptotic analysis to reveal this is different than the one we performed earlier in studying the long time approach of the PDF core to its invariant limit and it will be discussed in Sect. 7 in the context of a special class of initial cut-off.

6 Asymptotics of the Tracer PDF (4.5)

6.1 Core Behavior of $P_{\bar{T}}(\bar{T})$ ($\bar{T} \to 0$)

It is known from Sect. 4 that

$$P_{\bar{T}}(\bar{T}) = \frac{1}{\sqrt{2\pi}} \int_0^\infty \frac{e^{-\frac{\bar{T}^2}{2\sigma^2}} P_\eta(\eta)}{\sigma} d\eta. \tag{6.1}$$

For $|\bar{T}| \ll 1$, we can expand the exponential $e^{-\frac{\bar{T}^2}{2\sigma^2}}$ and a term-by-term integration leads to

$$P_{\bar{T}}(\bar{T}) = \sum_{n=0}^{\infty} \frac{(-1)^n \langle \sigma^{-2n-1} \rangle_\eta}{2^n\, n!} \bar{T}^{2n}, \quad \bar{T} \to 0, \tag{6.2}$$

given that $\langle \sigma^{-2n-1} \rangle_\eta = \int_0^\infty \sigma^{-2n-1} P_\eta(\eta) d\eta$ exists for $n = 0, 1, 2, \ldots$ and the above series converges. For smooth initial cut-off $\hat{\phi}_0$, (6.2) generally holds. In particular, for the invariant measure (5.4) for which we utilize $\sigma \propto \eta^{-\frac{\alpha+1}{4}}$ at long times from (6.7) and (6.15), $\langle \sigma^{-2n-1} \rangle_\eta$ exists for any n and its asymptotic approximation yields

$$\langle \sigma^{-2n-1} \rangle_\eta \sim n^{\frac{\alpha+1}{2} n + \frac{\alpha+1}{4}} e^{-\frac{\alpha+1}{2} n [1 - 2\ln 2 + 2\ln \pi - \ln(\alpha+1)]}, \quad n \to \infty, \tag{6.3}$$

up to some constant factor as a function of α only. Therefore, a ratio test shows that the series (6.2) has a radius of convergence of $e^{-1/2}$ when $\alpha \le 1$ and thus $P_{\bar{T}}(\bar{T})$ is analytic at $\bar{T} = 0$. Although the series fails to converge for $\alpha > 1$, the Dominated Convergence Theorem still guarantees that the derivative of any finite order exists at $\bar{T} = 0$ for $P_{\bar{T}}(\bar{T})$. Essentially, the algebraic growth of σ^{-2n-1} is dominated by the exponential decay of $P_\eta(\eta)$ for η large. To summarize, this differentiability essentially implies that the PDF remains *Gaussian* at the core: It is locally quadratic, although its value is larger than the core of the initial Gaussian measure, $(2\pi)^{-1/2}$. This contradicts the conjecture that the stretched exponential tails $Ae^{-B|\bar{T}|^{\frac{4}{3+\alpha}}}$, which would imply non-differentiability at $\bar{T} = 0$, extend to the core. Figure 9 illustrates the core and tail behavior of the invariant measure (5.4) for three different values of α, where the inset figures show the Gaussian (quadratic) behavior near the core. Notice that the widths of these quadratic regions are on the order of 1, 10^{-3} and 10^{-6}, respectively, because of the fact that the expansion coefficients (6.3) are increasing with respect to α. However, when σ^{-1} grows faster in η than the decay rate (9.7) of $P_\eta(\eta)$ and thus $\langle \sigma^{-2n-1} \rangle_\eta$ diverges for $n \ge 0$, the tracer PDF is singular at the core $\bar{T} = 0$. Consequently, we would not be able to obtain the series expansion (6.2) in such a case. An example will be given in Sect. 7, where $\hat{\phi}_0^2(k) = \delta(|k| - m)$ with the constant $M > 0$, so that

$$\sigma^{-1} = \frac{\exp(\frac{4\pi^2 m^2 t^2 \eta}{\mathrm{Pe}})}{(\cosh(4\pi m \sqrt{\frac{1}{\mathrm{Pe}}}\, t)^{\frac{1}{4}}}. \tag{6.4}$$

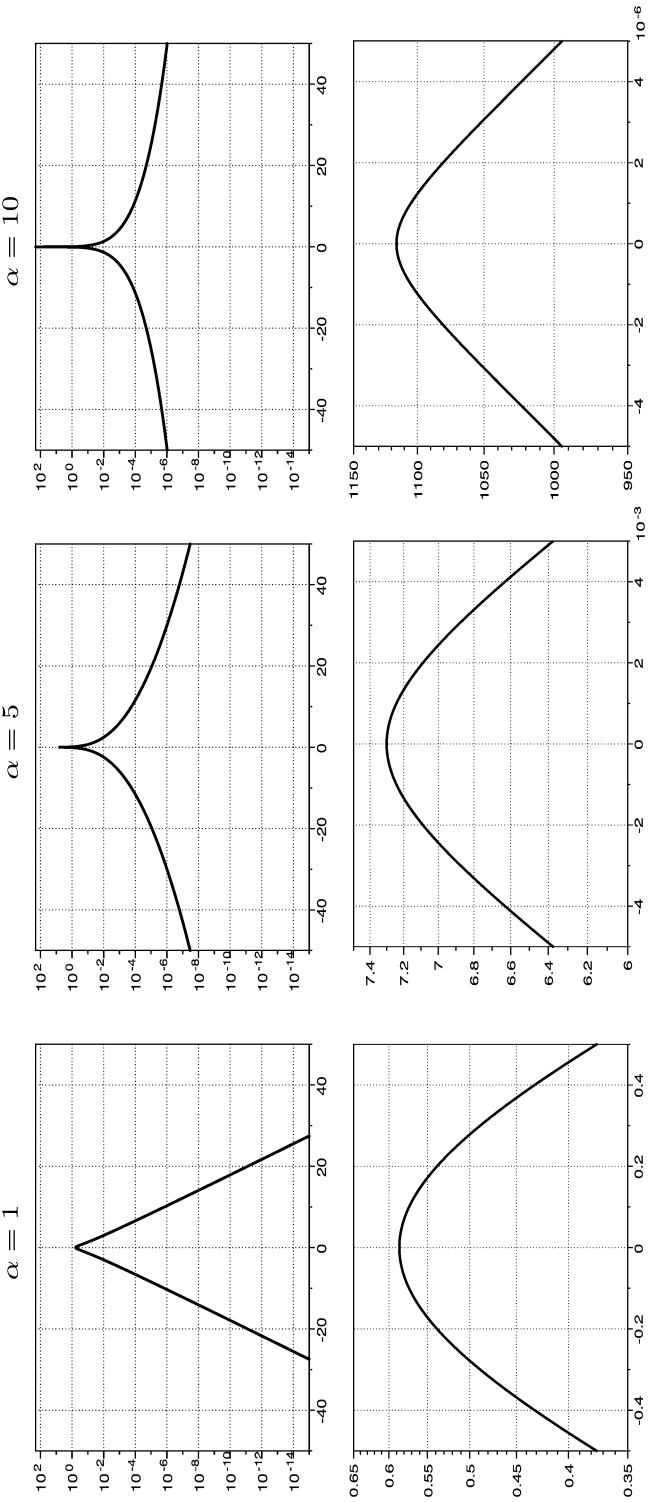

Fig. 9 Tail and core behavior of the invariant PDF (3.8) for different α

6.2 Long Time Asymptotics for $P_{\bar{T}}(\bar{T})$ in the Diffusionless Limit ($\mathrm{Pe} \to \infty$)

We now consider the scaling $t = (\mathrm{Pe})^{\theta}$ with $\theta > 0$, so that $t \to \infty$ when $\mathrm{Pe} \to \infty$.

1. $\theta < \frac{1}{2}$. Substitute the scaling ansatz in (4.2–4.4) and we have

$$\begin{aligned}\sigma^2 &= \frac{\int_{-\infty}^{\infty} |k|^{\alpha} \hat{\phi}_0^2(k) e^{-8\pi^2 k^2 [(\mathrm{Pe})^{\theta-1} + (\mathrm{Pe})^{2\theta-1}\eta]} dk}{\int_{-\infty}^{\infty} \frac{|k|^{\alpha} \hat{\phi}_0^2(k) e^{-8\pi^2 k^2 (\mathrm{Pe})^{\theta-1}\eta}}{\sqrt{\cosh(4\pi\sqrt{(\mathrm{Pe})^{2\theta-1}}k)}} dk} \\ &\to \frac{\int_{-\infty}^{\infty} |k|^{\alpha} \hat{\phi}_0^2(k) dk}{\int_{-\infty}^{\infty} |k|^{\alpha} \hat{\phi}_0^2(k) dk} = 1, \end{aligned} \tag{6.5}$$

as $\mathrm{Pe} \to \infty$ since in this limit, both $(\mathrm{Pe})^{\theta-1}$ and $(\mathrm{Pe})^{2\theta-1}$ vanish. Therefore

$$P_{\bar{T}}(\bar{T}) \sim \frac{1}{\sqrt{2\pi}} e^{-\frac{\bar{T}^2}{2}} \int_{-\infty}^{\infty} P_{\eta}(\eta) d\eta = \frac{1}{\sqrt{2\pi}} e^{-\frac{\bar{T}^2}{2}} \tag{6.6}$$

and $\bar{T}$ remains asymptotically a Gaussian Random Field in this time scale. It is also clear that in this limit the diffusion is effectively neglected and the random advection does not change the initial statistical distribution of the tracer.

2. $\theta > \frac{1}{2}$. First we consider the case where $\frac{1}{2} < \theta < 1$. In this time scale, $\frac{t}{\mathrm{Pe}} = (\mathrm{Pe})^{\theta-1} \to 0$ and $\frac{t^2}{\mathrm{Pe}} = (\mathrm{Pe})^{2\theta-1} \to \infty$ as $\mathrm{Pe} \to \infty$. Thus

$$\begin{aligned}\sigma^2 &\to \frac{\int_{-\infty}^{\infty} |k|^{\alpha} \hat{\phi}_0^2(k) e^{-8\pi^2 k^2 (\mathrm{Pe})^{2\theta-1}\eta} dk}{\int_{-\infty}^{\infty} \frac{|k|^{\alpha} \hat{\phi}_0^2(k)}{\sqrt{\cosh(4\pi\sqrt{(\mathrm{Pe})^{2\theta-1}}k)}} dk} \\ &\to \frac{2^{\frac{\alpha-1}{2}} \Gamma(\frac{\alpha+1}{2})}{\int_0^{\infty} \frac{u^{\alpha} du}{\sqrt{\cosh u}}} \eta^{-\frac{\alpha+1}{2}} \\ &= [C(\alpha)\, \eta^{\frac{\alpha+1}{2}}]^{-1} \end{aligned} \tag{6.7}$$

by applying Watson's Lemma. Furthermore, a very similar calculation generalizes this result for the case where $\theta \geq 1$. Substituting σ^2 in (4.5) with its asymptotic approximation (6.7) yields formula (5.4). Furthermore, by noticing that $P_{\eta}(\eta) \sim \frac{1}{2\sqrt{\pi\eta^3}} e^{-\frac{1}{8\eta}}$ as $\eta \to 0$, for large $\bar{T}$ we have

$$P_{\bar{T}}(\bar{T}) \sim \frac{\sqrt{C(\alpha)}}{2\sqrt{2}\,\pi} \int_0^{\varepsilon} \eta^{\frac{\alpha+1}{4} - \frac{3}{2}} e^{-\frac{\bar{T}^2}{2} C(\alpha) \eta^{\frac{\alpha+1}{2}} - \frac{1}{8\eta}} d\eta \tag{6.8}$$

for a small, fixed ε. To determine where this integral is dominated, we can solve the equation

$$\psi'(\eta) = \frac{d}{d\eta}\left(\bar{T}^2 C(\alpha) \eta^{\frac{\alpha+1}{2}} + \frac{1}{8\eta}\right) = 0 \tag{6.9}$$

and we have $\eta = \tilde{C}(\alpha)|\bar{T}|^{-\frac{4}{3+\alpha}}$. Then the change of variable $\eta = s|\bar{T}|^{-\frac{4}{3+\alpha}}$ in (6.8) leads to a standard Laplace integral and its asymptotic expansion reads

$$P_{\bar{T}}(\bar{T}) \sim A(\alpha)|\bar{T}|^{-\frac{\alpha+1}{\alpha+3}} e^{-B(\alpha)|\bar{T}|^{\frac{4}{\alpha+3}} + o(|\bar{T}|^{\frac{4}{\alpha+3}})}, \quad |\bar{T}| \to \infty, \tag{6.10}$$

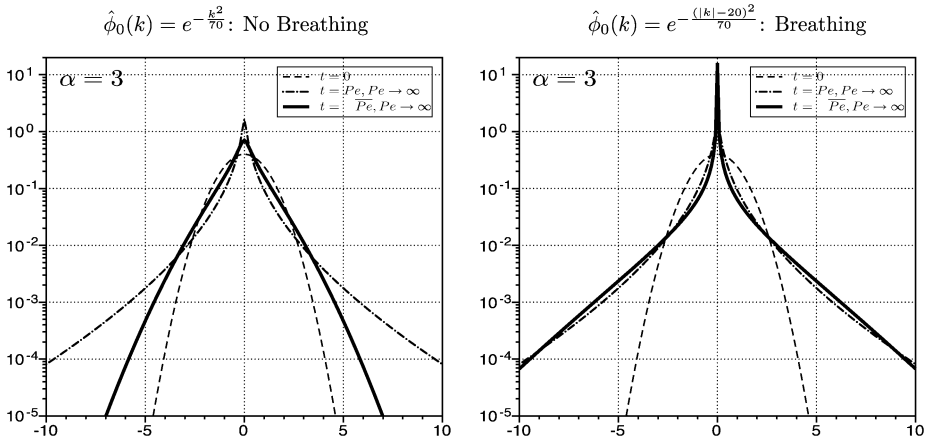

Fig. 10 Long time PDFs for different $\hat{\phi}_0(k)$, where $\alpha = 3$, $\mathrm{Pe} \to \infty$: new long time, invariant measure in the diffusionless limit

where A and B are constant functions of α only. Thus, this PDF has a stretched exponential tail, which is exactly the one recovered in previous work [7, 8, 28], namely, the measure (3.8). The significance of the present analysis lies in the distinguished scaling between t and $\frac{1}{\mathrm{Pe}}$ that it reveals.

3. $\theta = \frac{1}{2}$. In this critical time scale,

$$\sigma^2 \to \frac{\int_{-\infty}^{\infty} |k|^\alpha \hat{\phi}_0^2(k) e^{-8\pi^2 k^2 \eta} dk}{\int_{-\infty}^{\infty} \frac{|k|^\alpha \hat{\phi}_0^2(k)}{\sqrt{\cosh(4\pi k)}}\, dk}. \tag{6.11}$$

The ensuing PDF (6.1) is special in the sense that we cannot further approximate the conditional variance and it suggests nontrivial dependence on the initial cut-off function, $\hat{\phi}_0(k)$. The numerical results shown in Fig. 10 suggest that this scaling, $t = \sqrt{\mathrm{Pe}}$ as $\mathrm{Pe} \to \infty$, corresponds to the "breathing" PDF described in Sect. 5.4. Here the initial Gaussian ($t = 0$) and the invariant measure (6.10) ($t = \mathrm{Pe}$ and $\mathrm{Pe} \to \infty$) are also plotted for comparison. Therefore, this is a *new* long time invariant measure in the diffusionless limit, different from the measure (6.10), and its existence is completely determined by the initial cut-off function $\hat{\phi}_0$. In particular, when breathing occurs for $\hat{\phi}_0(k) = e^{-\frac{(|k|-20)^2}{70}}$, for some intermediate values of $\bar{T}$, the measure has a larger concavity than the initial Gaussian and the measure (6.10); $P_{\bar{T}}(0)$ is largest when $t = \sqrt{\mathrm{Pe}}$ and $\mathrm{Pe} \to \infty$, which is consistent with the characteristics discussed in Sect. 5.4.

The anomalies in the PDF concavity and the zero fluctuation density, $P_{\bar{T}}(0)$, shown in Fig. 10, together change the relationship between the new invariant measure and the invariant measure (3.8): As $|\bar{T}|$ increases from 0, the new invariant measure exhibits "larger→smaller→ larger→smaller" behavior compared to the measure (6.10), when breathing occurs in the right panel, whereas in the left panel the transition has only three phases, "smaller→larger→ smaller". This adds another characterization of the breathing phenomenon which can also be inferred from Fig. 4, though the phase where the breathing PDF is smaller than the invariant measure in the tails is not shown.

Next we study the tail asymptotics of the tracer PDF in this regime and see if it is different from Gaussian and the stretched exponential (6.10). First consider the spe-

cial case when $\hat{\phi}_0(k) = \exp(-\frac{\pi^2 k^2}{2V})$ with V as a constant determining the spread of the random spectrum of the initial random field. Then (6.11) can be simplified, since $\sigma^2 \to (A + B\eta)^{-\frac{\alpha+1}{2}}$ as $\mathrm{Pe} \to \infty$, where

$$\begin{aligned} A &= A(V,\alpha) = \pi^2 V^{-1}\left(\int_{-\infty}^{\infty} \frac{|k|^\alpha \hat{\phi}_0^2(k)}{\sqrt{\cosh(4\pi k)}}\,dk\right)^{\frac{2}{\alpha+1}}, \\ B &= B(V,\alpha) = 8\pi^2\left(\int_{-\infty}^{\infty} \frac{|k|^\alpha \hat{\phi}_0^2(k)}{\sqrt{\cosh(4\pi k)}}\,dk\right)^{\frac{2}{\alpha+1}}. \end{aligned} \tag{6.12}$$

By letting $s = \frac{B}{A}\eta = 8V\eta$, we claim that for large $|\bar{T}|$ the probability density (6.1) is approximated by

$$P_{\bar{T}}(\bar{T}) \sim \frac{A^{\frac{\alpha+1}{4}}\sqrt{V}}{\pi}\int_0^{\varepsilon} \sqrt{\frac{(1+s)^{\frac{\alpha+1}{2}}}{s^3}}\,\exp\left[-x(1+s)^{\frac{\alpha+1}{2}} - \frac{V}{s}\right]ds, \tag{6.13}$$

where $x = \frac{\bar{T}^2 A^{\frac{\alpha+1}{2}}}{2}$. Here, $\varepsilon \ll 1$ is fixed so that $P_\eta(\eta) \sim \frac{1}{2\sqrt{\pi\eta^3}}\,e^{-\frac{1}{8\eta}}$ when $\eta \le \varepsilon$. The above integral is again a Laplace integral with a movable maximum and its asymptotic approximation reads

$$P_{\bar{T}}(\bar{T}) \sim \frac{\sqrt{\tilde{A}}}{e^{\frac{V(\alpha-1)}{4}}\sqrt{\pi}}\,e^{-\frac{\tilde{A}}{2}\bar{T}^2 - \sqrt{\tilde{A}V(\alpha+1)}\,|\bar{T}|}\left(1 + \frac{(\alpha+3)\sqrt{2V}}{48\sqrt{(\alpha+1)x}}[6 + V(\alpha-1)]\right), \tag{6.14}$$

when $|\bar{T}| \to \infty$ and $\tilde{A} = A^{\frac{\alpha+1}{2}}$. Thus, this PDF still has a Gaussian tail, which is different from that of the unit Gaussian at $t = 0$. Although the explicit formula for σ^2 is not available when $\hat{\phi}_0(k) = e^{-\frac{(|k|-20)^2}{70}}$, which is more relevant to the breathing phenomena, numerical results suggest that the induced PDF also has Gaussian tails similar to (6.14).

6.3 Tail Asymptotics for $P_{\bar{T}}(\bar{T})$ ($\bar{T} \to \infty$) at Large Times for Finite, Non-Zero Pe

It was noted by Bronski and McLaughlin [7, 8] and Vanden-Eijnden [28] that at finite times, for fixed $\mathrm{Pe} \neq 0$, the PDF tail is Gaussian with outward propagating non-Gaussianity, in particular given by the stretched exponential regime (3.8). Here we provide a sharp estimate of the speed of such propagation as a function of time.

Letting $\beta = \frac{\alpha+1}{2} > 0$, a similar calculation as in (6.7) reads

$$\sigma^2 \sim \left[C(\alpha)\left(\eta + \frac{1}{t}\right)^\beta\right]^{-1} \tag{6.15}$$

for finite, non-vanishing Pe, where $C(\alpha)$ is defined in (5.12). Therefore, in this case

$$P_{\bar{T}}(\bar{T}) \sim \frac{\sqrt{\widetilde{C}(\beta)}}{2\sqrt{2}\,\pi}\int_0^{\varepsilon} \sqrt{\frac{(\eta+\frac{1}{t})^\beta}{\eta^3}}\,\exp\left[-\frac{\bar{T}^2}{2}\widetilde{C}(\beta)\left(\eta+\frac{1}{t}\right)^\beta - \frac{1}{8\eta}\right]d\eta \tag{6.16}$$

for large $|\bar{T}|$. Notice that there are two large parameters in (6.16), namely, the magnitude of the renormalized tracer $|\bar{T}|$ and the time t. If we first let t go to infinity, then (6.16) formally reduces to (6.8) and this corresponds to the tail asymptotics of the long time, stationary

tracer PDF with finite diffusivity [6, 28]. In other words, in the $(1/t, 1/|\bar{T}|)$ plane, this limiting procedure is equivalent to approaching the origin along the $1/|\bar{T}|$-axis.

Alternatively, next we consider the singular limit along the curve $\widetilde{C}(\beta)|\bar{T}|^2 = 2t^{2\gamma}$ with $\gamma > 0$. Then (6.16) becomes

$$P_{\bar{T}}(\bar{T}) \sim \frac{\sqrt{\widetilde{C}(\beta)}}{2\sqrt{2}\,\pi}\, e^{-t^{2\gamma-\beta}} \int_0^{\varepsilon} \sqrt{\frac{(\eta+\frac{1}{t})^{\beta}}{\eta^3}} \exp\left\{-t^{2\gamma-\beta}[(t\eta+1)^{\beta}-1] - \frac{1}{8\eta}\right\} d\eta. \quad (6.17)$$

Again, this is a Laplace integral with a movable maximum and we have to solve the algebraic equation

$$\frac{\partial}{\partial \eta}\left\{t^{2\gamma-\beta}[(t\eta+1)^{\beta}-1] + \frac{1}{8\eta}\right\} = 0 \quad (6.18)$$

to determine where the dominant contribution localizes near $\eta = 0$. Next we consider two different cases:

Case 1: $2\gamma - \beta \le 1$, or equivalently, $\gamma \le \frac{\beta+1}{2} = \frac{\alpha+3}{4}$. In this case, using the Method of Dominant Balance for $\gamma < \frac{\beta+1}{2}$, we have

$$\eta \sim (8\beta)^{-\frac{1}{1+\beta}} t^{-\frac{2\gamma}{1+\beta}} \quad (6.19)$$

since $t\eta \propto t^{\frac{\beta-2\gamma+1}{1+\beta}} \gg 1$ when t is large. Moreover, this result also applies when $\gamma = \frac{\beta+1}{2}$ and thus $t\eta = O(1)$. Then the change of variable $\eta = s(8\beta)^{-\frac{1}{1+\beta}} t^{-\frac{2\gamma}{1+\beta}}$ reproduces very similar calculations as in (6.8) through (6.10) and the result reads

$$P_{\bar{T}}(\bar{T}) \sim A_1(\alpha,\gamma)|\bar{T}|^{-\frac{\alpha+1}{\alpha+3}} e^{-B_1(\alpha,\gamma)|\bar{T}|^{\frac{4}{\alpha+3}} + o(|\bar{T}|^{\frac{4}{\alpha+3}})} \quad (6.20)$$

for $|\bar{T}|$ large, where $A_1(\alpha,\gamma)$ and $B_1(\alpha,\gamma)$ are functions of α and γ alone. Notice that here $|\bar{T}|^{\frac{4}{\alpha+3}} = t^{\frac{2\gamma}{1+\beta}} \ge t^{2\gamma-\beta}$ and therefore the $e^{-t^{2\gamma-\beta}}$ term in the prefactor of (6.17) doesn't affect the asymptotic result (6.20).

Case 2: $2\gamma - \beta > 1$, or equivalently, $\gamma > \frac{\alpha+3}{4}$. In this case, solving (6.18) implies

$$\eta \sim \frac{1}{\sqrt{8\beta}} t^{\frac{\beta-1}{2}-\gamma} \quad (6.21)$$

since here $t\eta \propto t^{1-\gamma+\frac{\beta-1}{2}} \ll 1$ when t is large. Thus, the asymptotic approximation to (6.17) reads

$$P_{\bar{T}}(\bar{T}) \sim A_2(\alpha,\gamma)\bar{T}^{\frac{1}{2}-\frac{1+3\alpha}{8\gamma}} e^{-B_2(\alpha,\gamma)|\bar{T}|^{2-\frac{\alpha+1}{2\gamma}} + o(|\bar{T}|^{2-\frac{\alpha+1}{2\gamma}})}, \quad |\bar{T}| \to \infty. \quad (6.22)$$

This is also "heavier" than Gaussian, since $\alpha + 1 > 0$, but "lighter" than the stretched exponential shown in (6.20).

The results (6.20) and (6.22) suggest that as time advances, the stretched exponential regime in the renormalized tracer PDF propagates towards the tail of the PDF at a critical algebraic rate proportional to $t^{\frac{\alpha+3}{4}}$. However, for the values of $|\bar{T}|$ growing in faster algebraic rates with respect to time, the corresponding region in the PDF also exhibits heavy-tailed behavior, which is an intermediate state between Gaussian and the tail behavior of the long time stationary PDF.

It should be noted that similar to the asymptotic calculations done in Sect. 5.4, the asymptotic analysis of $P_{\bar{T}}(\bar{T})$ in this section is derived from the pointwise asymptotic approximation of σ^2 in terms of η, which is uniform in any compact subset of $(0,\infty)$. Nonetheless, excluding the set of measure zero (the point $\eta = 0$) in the integration is justified by the super-exponential decay of $P_\eta(\eta)$ and the rigorous proof is not pursued in this paper.

7 Discussion of the Condition for the "Breathing"

As we saw in the numerical results in Sect. 5, the "breathing" phenomenon is characterized by the non-monotonic behavior of the renormalized tracer PDF in time. We further defined that a "breathing" occurs when $P_{\bar{T}}(\bar{0})$ exceeds its invariant limit at least once. We also saw with fixed Pe, how the bimodality of $\hat{\phi}_0$ introduced by its *local* concavity near $k = 0$ preserves the signature of breathing at long time. Nonetheless, the breathing at finite, short times observed in Figs. 3, 4, 5 and 6 cannot be recovered by this long time asymptotics.

Alternatively, in Sect. 6 we reproduced the characteristics of the short time breathing through proper asymptotic limiting procedure. From the difference between the two types of $\hat{\phi}_0$ we chose, it is natural to conjecture that the breathing of PDF might be related to the non-monoticity of $\hat{\phi}_0(k)$ as $|k|$ varies. However, the rigorous analysis to show how breathing at short times depends on general bimodality in the cut-off is very complicated, given the integral forms of the variances and $P_\eta(\eta)$ in Sect. 4. Recall that the PDF breathes if the PDF core has a temporal maximum exceeding its invariant limit. In this section we illustrate how such a maximum can be established at short time by choosing special $\hat{\phi}_0(k)$ given by Dirac delta functions so that the variance (4.4) can be computed in explicit closed form expressions.

From Sect. 4, we can derive

$$\begin{aligned}\frac{\partial}{\partial t}P_{\bar{T}}(\bar{T}) &= \frac{1}{\sqrt{2\pi}}\int_0^\infty \frac{\partial}{\partial t}\left(\frac{e^{-\frac{\bar{T}^2}{2\sigma^2}}}{\sigma}\right)P_\eta(\eta)d\eta \\ &= \frac{1}{2\sqrt{2\pi}}\int_0^\infty \frac{e^{-\frac{\bar{T}^2}{2\sigma^2}}}{\sigma^5}(\bar{T}^2-\sigma^2)\frac{\partial}{\partial t}(\sigma^2)P_\eta(\eta)d\eta.\end{aligned}$$

Clearly, if $\frac{\partial}{\partial t}(\sigma^2)$ is sign definite for any t and η, then so is $\frac{\partial}{\partial t}P_{\bar{T}}(0)$ and thus $P_{\bar{T}}(0)$ is monotonic. Similarly, since $\sigma^2(t,\eta) \le \sigma^2(t,0)$, for $|\bar{T}| \ge \sigma(t,0)$ from (4.2) uniform monotonicity of σ^2 also implies the monotonicity of $P_{\bar{T}}(\bar{T})$. Of course, it is too restrictive to impose uniform monotonicity on σ^2 for general t and η; from the previous figures, we know that $P_{\bar{T}}(0)$ attains a local temporal maximum when breathing occurs, while it is monotonically increasing if there is no breathing. To illustrate how such monotonicity in $P_{\bar{T}}(0)$ can be established, we consider a simple example by using the initial cut-off function $\hat{\phi}_0^2(k) = \delta(|k|-m)$ with the constant $m > 0$, so that

$$\sigma^2(t,\eta) = \left(\cosh\left(4\pi m t\sqrt{\frac{1}{\mathrm{Pe}}}\right)\right)^{-\frac{1}{2}}\exp\left(-\frac{8\pi^2 m^2 t^2 \eta}{\mathrm{Pe}}\right),$$

which can be easily verified from the definitions (4.2–4.4). To show that $P_{\hat{T}}(0)$ is constantly increasing, it suffices to show that

$$\int_0^\infty e^{\xi\eta}\left(\eta-\frac{1}{2}\right)P_\eta(\eta)d\eta > 0 \tag{7.1}$$

for any $\xi > 0$ since in this case

$$\begin{aligned}\frac{\partial}{\partial t}P_{\bar{T}}(0) &= \frac{1}{\sqrt{2\pi}}\int_0^\infty \frac{\partial}{\partial t}\left(\frac{1}{\sigma}\right)P_\eta(\eta)d\eta \\ &= \frac{\xi}{t\sqrt{2\pi\sqrt{\cosh(2\sqrt{\xi})}}}\int_0^\infty e^{\xi\eta}\left(\eta - \frac{\tanh(2\sqrt{\xi})}{4\sqrt{\xi}}\right)P_\eta(\eta)d\eta \\ &\geq \frac{\xi}{t\sqrt{2\pi\sqrt{\cosh(2\sqrt{\xi})}}}\int_0^\infty e^{\xi\eta}\left(\eta - \frac{1}{2}\right)P_\eta(\eta)d\eta \end{aligned} \tag{7.2}$$

with $\xi = 4\pi^2 M^2 \frac{1}{\mathrm{Pe}} t^2 > 0$. To prove (7.1), one only needs to realize that

$$\int_0^\infty e^{\xi\eta}\left(\eta - \frac{1}{2}\right)P_\eta(\eta)d\eta > e^{\xi/2}\int_0^\infty \left(\eta - \frac{1}{2}\right)P_\eta(\eta)d\eta = 0, \tag{7.3}$$

since

$$\int_0^\infty \eta P_\eta(\eta)d\eta = \langle\eta\rangle = -\frac{\partial}{\partial s}\frac{1}{\sqrt{\cosh\sqrt{2s}}}\bigg|_{s=0} = \frac{1}{2}. \tag{7.4}$$

Next we consider a slightly different type of cut-off function with energy spectrum concentrated at two wavenumbers, namely,

$$\hat{\phi}_0^2(k) = \delta(|k| - m) + R\delta(|k| - cm) \tag{7.5}$$

for which one can observe breathing for some combinations of values of positive constants m, c and R. In this case, the explicit formula for the conditional variance is also available via

$$\sigma^2(\eta, t) = \frac{e^{-2M^2(t+t^2\eta)} + Rc^\alpha e^{-2c^2M^2(t+t^2\eta)}}{\frac{e^{-2M^2t}}{\sqrt{\cosh(2Mt)}} + Rc^\alpha \frac{e^{-2c^2M^2t}}{\sqrt{\cosh(2cMt)}}} \tag{7.6}$$

with $M = 2\pi m\sqrt{\frac{1}{\mathrm{Pe}}}$. To reduce the complexity of exploring the four-dimensional (M, c, R, α) parameter space, we first take the asymptotic limit $c \to 0$ requiring finite $Rc^\alpha \equiv L > 0$, which implies that $R \to 0$ if $-1 < \alpha < 0$, $R \to \infty$ if $\alpha > 0$ and $R \equiv 1$ if $\alpha = 0$. Thus, the conditional variance (7.6) is reduced to

$$\sigma^2(\eta, t) \to \frac{e^{-2M^2(t+t^2\eta)} + L}{\frac{e^{-2M^2t}}{\sqrt{\cosh(2Mt)}} + L}, \quad c \to 0. \tag{7.7}$$

With this expression for σ^2, the numerical integration shows that the breathing phenomenon occurs at a time scale proportional to $\frac{1}{M^2}$ for large M, thus next we study the large M asymptotics of

$$\frac{\partial}{\partial t}P_{\bar{T}}(0) = \frac{1}{\sqrt{2\pi}}\int_0^\infty \frac{\partial}{\partial t}\left(\frac{e^{-2M^2(t+t^2\eta)} + L}{\frac{e^{-2M^2t}}{\sqrt{\cosh(2Mt)}} + L}\right)^{-\frac{1}{2}} P_\eta(\eta)d\eta \tag{7.8}$$

at $t = \frac{l}{M^2}$ with some constant $l > 0$. This identifies quantitatively the "breathing" non-monotonic behavior of the tracer PDF. After some algebra, (7.8) is expanded into

$$\frac{\partial}{\partial t} P_{\bar{T}}(0)\Big|_{t=\frac{l}{M^2}} = \frac{Me^{-l}}{2\sqrt{2\pi(e^{-2l} + L\sqrt{\cosh\frac{2l}{M}})}} \sum_{i=1}^{3} g_i(M) \int_0^\infty h\left(\frac{\eta}{M^2}\right) f_i\left(\frac{\eta}{M^2}\right) P_\eta(\eta)d\eta, \tag{7.9}$$

where $h = e^{\frac{l^2\eta}{M^2}}(1 + Le^{2l(1+\frac{l\eta}{M^2})})^{-\frac{3}{2}}$ and

$$\begin{aligned} &g_1 = 2MLe^{2l}\sqrt{\cosh\tfrac{2l}{M}}, \quad && g_2 = 2M, && g_3 = -\tanh\tfrac{2l}{M}, \\ &f_1 = 1 + \tfrac{2l\eta}{M^2}, && f_2 = \tfrac{2l\eta}{M^2} - Le^{2l(1+\frac{l\eta}{M^2})}, && f_3 = 1 + Le^{2l(1+\frac{l\eta}{M^2})}. \end{aligned} \tag{7.10}$$

We observe that $hf_i, i = 1, 2, 3$ are all smooth bounded functions on $[0, \infty]$. Thus we can expand each of them into a power series of $\frac{\eta}{M^2}$, followed by a term-by-term integration to evaluate each of the three integrals in (7.9) utilizing

$$\int_0^\infty \left(\frac{\eta}{M^2}\right)^n P_\eta(\eta)d\eta = M^{-2n}\langle\eta^n\rangle = (-1)^n n! M^{-2n} \frac{\partial^n}{\partial s^n} \frac{1}{\sqrt{\cosh\sqrt{2s}}}\Big|_{s=0}. \tag{7.11}$$

In fact, the above analysis can be generalized to $\bar{T} \neq 0$ and ultimately we have

$$\frac{\partial}{\partial t} P_{\bar{T}}(\bar{T})\Big|_{t=\frac{l}{M^2}} = \frac{l^3 e^{-\frac{\bar{T}^2}{2}}[1 + L(1-l)e^{2l}](3 - 6\bar{T}^2 + \bar{T}^4)}{3\sqrt{2\pi}\,(1 + Le^{2l})^3} M^{-2} + O(M^{-4}), \quad M \to \infty. \tag{7.12}$$

Therefore, for large M, the sign of $\frac{\partial}{\partial t} P_{\bar{T}}(\bar{T})$ is determined by that of $[1 + L(1-l)e^{2l}](3 - 6\bar{T}^2 + \bar{T}^4)$. Moreover, it is straightforward to see that the equation $1 + L(1-l)e^{2l} = 0$ has one and only one positive root $l^* = l^*(L)$ for fixed $L > 0$, which in turn suggests that with the cut-off function (7.5) breathing will occur around $t = t^* = M^{-2}l^*(L) = M^{-2}l^*(Rc^\alpha)$ for large M in the limit $c \to 0$ and $Rc^\alpha \equiv L$. In particular, for $\bar{T}^2 \in [0, 3 - \sqrt{6}) \cap (3 + \sqrt{6}, \infty)$, $P_{\bar{T}}(\bar{T})$ has exactly one temporal maximum; otherwise, $P_{\bar{T}}(\bar{T})$ has exactly one temporal minimum.

8 Conclusions and Future Work

The integral formalism presented in this paper offers a comprehensive picture of the evolution of the Majda model which had previously been only analyzed in the tail at long times, or from statistical moments. Through this formulation, we have documented a new breathing phenomenon which occurs when there are multiple peaks in the initial scalar correlation function. We have documented this behavior both numerically and analytically.

Further, we have presented a detailed description of the invariant measure by establishing that it always has a Gaussian core, distinguished from the stretched exponential tail in that the core is infinitely differentiable (but not necessarily analytic), whereas a pure stretched exponential distribution is not. Moreover, a joint distinguished limit of time and Péclet number identifies a breathing PDF as a new invariant measure. Additionally, we calculated the explicit rate of approach in time to the invariant heavy tail. Lastly, by introducing a class of special data exact results that predict the occurrence of the breathing phenomenon have been derived.

Future directions include the assessment of initial data possessing a non-trivial mean as well exploration of multi-point and gradient statistics. Further work will consider the role of an additional deterministic linear shear layer, which Majda examined for finite moments [16], as these flows may give rise to interesting transient dynamics in the PDF such as those observed here. Additionally, with the complete analysis now available for the Majda model, a future direction worth exploring is the comparison between the predictions of the Majda model and other more general random flows, such as Batchelor or Kraichnan models. Much less is known about those models. In the decaying case, calculations by Balkovsky and Fouxon [2] suggest divergent scalar factors for Batchelor flows, and gradient statistics with similar long time, flatness factors. Divergent flatness factors have also been reported in the Majda model, by Majda, and McLaughlin and Majda, but for a class of random wave initial data. Further, Bronski and McLaughlin [8] established that the statistics of derivatives in the shear direction for the Majda model are different from the scalar statistics, with a precise relation of the stretching exponents, while they reported that the derivatives in the cross-shear direction share the same statistics as the scalar itself. In the pumped case, it was reported by Chertkov et al. [10–12] that the gradient statistics in the Batchelor case have statistics with heavier tails than the scalar statistics themselves, similar to the shear derivatives in the Majda model, and also similar to various numerical [14], and experimental observations [13, 27]. The varying predictions in these more general flows suggest that the complete analysis of the entire PDF presented here for the Majda model may provide a starting point for a better understanding of the general turbulent scalar statistics.

Acknowledgements The authors thank Jared C. Bronski for helpful discussions. RMM and ZL were partially supported by a National Science Foundation Collaborations in Mathematical Geosciences (CMG) Award, NSF ATM-0327906. RMM was also partially supported by NSF DMS-030868. RC was partially supported by NSF DMS-0104329 and DMS-0509423. Computational work was supported by DMS-SCREMS 0422417.

Appendix

9.1 The Numerical Integration of $P_\eta(\eta)$

Recall that $\eta := \int_0^1 B^2(s)ds$. Although we do not know the explicit formula for $P_\eta(\eta)$, the probability density function for the L^2 norm of the Wiener process $B(t)$, its Laplace transform is known explicitly and can be obtained by discretizing $B(t)$ by $B(t) \approx \sum_{i=1}^n \xi_i$, where $\xi_i,\ i = 1, 2, \ldots, n$ are i.i.d., mean-zero Gaussian random variables with variance $1/n$. Then by letting $n \to \infty$, it is known by solving an eigenvalue problem [6, 28] that

$$\langle e^{-s\eta}\rangle_\eta = \int_0^\infty e^{-s\eta} P_\eta(\eta)d\eta = \prod_{k=1}^\infty \left(1 + \frac{2s}{(k-\frac{1}{2})^2\pi^2}\right)^{-\frac{1}{2}} \tag{9.1}$$

for any $s > 0$. In other words, $P_\eta(\eta)$ can be represented as an inverse Laplace transform (4.6) assuming the convergence of the integral and the fact that the infinite product is defined to be analytic on the imaginary axis. The $-1/2$ powers in the infinite product expression (9.1), introduce multivaluedness that can be eliminated with a choice of branch cuts in the complex s-plane. Specifically, the choice of a branch cut for each square root in the product (9.1) along the negative real axis $(-\infty, 0]$ produces a function analytic everywhere in the complex plane cut along the line segments $\bigcup_{k=0}^\infty [-(2k+\frac{3}{2})^2\pi^2/2, -(2k+\frac{1}{2})^2\pi^2/2], k = 0, 1, \ldots$. This particular choice will, as we shall see, guarantee the convergence of the integral

for $\eta \neq 0$, and will allow us to transform the integration path from the imaginary axis into an infinite sum of line segments mentioned above on the negative real axis. Since $\prod_{k=1}^{\infty}(1+s^2(k-\frac{1}{2})^{-2}\pi^{-2})$ is the infinite product expansion for $\cosh s$, the infinite product in (4.6) can be expressed compactly via a cosh function, which then helps the numerical evaluation of this integral. Thus, the infinite product in (4.6) is simply $(\cosh\sqrt{2s})^{-1/2} = (-i)^{2k+1}(-\cos\sqrt{-2s})^{-1/2}$, and the Bromwich integral (4.6) reduces to a series of real integrals with terms that can be evaluated by numerical quadratures.

The above strategy requires $\eta > 0$ to guarantee the convergence of the series. When $\eta = 0$, we need to evaluate the Bromwich integral (4.6) directly along the imaginary axis. Alternatively, it follows from the small η asymptotic analysis shown in the Appendix 9.2 that

$$P_\eta(0) = 0. \tag{9.2}$$

9.2 The Asymptotics of $P_\eta(\eta)$

Next we discuss the behavior of $P_\eta(\eta)$ when $\eta \to 0^+$ and $\eta \to \infty$ utilizing (9.1) and (4.6). When $s \to +\infty$, the integral in (9.1) is a Laplace integral and the dominant contribution is

$$\int_0^{\varepsilon} e^{-s\eta} P_\eta(\eta) d\eta \tag{9.3}$$

with $\varepsilon \ll 1$, and it should be asymptotically approximated by $(\cosh\sqrt{2s})^{-1/2} \sim \sqrt{2}\exp(-\sqrt{\frac{s}{2}})$ for s large. However, if $P_\eta(\eta)$ has an integrable power series expansion near $\eta = 0$, a contradiction occurs since Watson's Lemma suggests that the leading asymptotics for $\mathbf{E}(e^{-s\eta})$ would be $s^{-\gamma}$ with $\gamma > 0$, which is a constant determined by the expansion. In light of this fact, we propose the ansatz that $P_\eta(\eta)$ has the following *super-exponential* asymptotic behavior near 0:

$$P_\eta(\eta) \sim A\eta^B \exp\left(-\frac{C}{\eta^D}\right), \quad \eta \to 0^+ \tag{9.4}$$

with $C, D > 0$. By substituting $P_\eta(\eta)$ in (9.3) with the right hand side in (9.4) and matching the constants, we find $A = \frac{1}{2\sqrt{\pi}}$, $B = -\frac{3}{2}$, $C = \frac{1}{8}$, and $D = 1$. Therefore

$$P_\eta(\eta) \sim \frac{1}{2\sqrt{\pi}\eta^3} e^{-\frac{1}{8\eta}}, \quad \eta \to 0^+. \tag{9.5}$$

When η is large, we notice that by choosing the branch cuts as suggested above, the Bromwich integral (4.6) can be evaluated by transforming the integration path into an infinite sum of closed contours each of which loops around one of the intervals $[-\frac{(2k+\frac{3}{2})^2\pi^2}{2}, -\frac{(2k+\frac{1}{2})^2\pi^2}{2}]$, $k = 0, 1, 2, \ldots$. The standard procedure of tightening the loops around the intervals yields

$$\begin{aligned} P_\eta(\eta) &= -\frac{1}{\pi i}\sum_{k=0}^{\infty}\int_{-\frac{(2k+\frac{3}{2})^2\pi^2}{2}}^{-\frac{(2k+\frac{1}{2})^2\pi^2}{2}} \prod_{j=1}^{\infty}\left(1+\frac{2s}{(j-\frac{1}{2})^2\pi^2}\right)^{-\frac{1}{2}} e^{s\eta} ds \\ &= \frac{1}{\pi}\sum_{k=0}^{\infty}\int_{\frac{(2k+\frac{1}{2})^2\pi^2}{2}}^{\frac{(2k+\frac{3}{2})^2\pi^2}{2}} \frac{(-1)^k e^{-t\eta} dt}{\sqrt{-\cos\sqrt{2t}}} \end{aligned}$$

$$= \frac{1}{\pi}\sum_{k=0}^{\infty}(-1)^k e^{-\frac{(2k+\frac{1}{2})^2\pi^2}{2}\eta}\int_0^{(2k+1)\pi^2}\frac{e^{-r\eta}dt}{\sqrt{-\cos\sqrt{2[r+(2k+1/2)^2\pi^2/2]}}}$$

$$\sim \frac{e^{-\frac{\pi^2}{8}\eta}}{\pi}\int_0^{\pi^2}\frac{e^{-t\eta}dt}{\sqrt{-\cos\sqrt{2t+\pi^2/4}}}, \quad \eta\to+\infty. \tag{9.6}$$

This is again a Laplace integral and a straightforward application of Watson's Lemma yields

$$P_\eta(\eta) \sim \frac{1}{\sqrt{2\eta}}e^{-\frac{\pi^2}{8}\eta}\left(1+\frac{1}{2\pi^2\eta}\right), \quad \eta\to+\infty. \tag{9.7}$$

References

1. Antonia, R.A., Sreenivasan, K.R.: Log-normality of temperature dissipation in a turbulent boundary layer. Phys. Fluids **20**, 1800–1804 (1977)
2. Balkovsky, E., Fouxon, A.: Universal long-time properties of Lagrangian statistics in the Batchelor regime and their application to the passive scalar problem. Phys. Rev. E **60**(4), 4164–4174 (1999)
3. Batchelor, G.K.: Small-scale variation of convected quantities like temperature in turbulent fluid, Part 1. General discussion and the case of small conductivity. J. Fluid Mech. **5**, 113–133 (1959)
4. Bender, C.M., Orszag, S.A.: Advanced Mathematical Methods for Scientists and Engineers: Asymptotic Methods and Perturbation Theory. Springer, New York (2005)
5. Bourlioux, A., Majda, A.J.: Elementary models with probability distribution function intermittency for passive scalars with a mean gradient. Phys. Fluids **14**, 881–897 (2002)
6. Bronski, J.C.: Asymptotics of Karhunen–Loeve eigenvalues and tight constants for probability distributions of passive scalar transport. Commun. Math. Phys. **238**(3), 563–582 (2003)
7. Bronski, J.C., McLaughlin, R.M.: Passive scalar intermittency and the ground state of Schrödinger operators. Phys. Fluids **9**, 181–190 (1997)
8. Bronski, J.C., McLaughlin, R.M.: Rigorous estimates of the tails of the probability distribution function for the random linear shear model. J. Stat. Phys. **98**(3–4), 897–915 (2000)
9. Castaing, B., Gunaratne, G., Heslot, F., Kadanoff, L., Libchaber, A., Thomae, S., Wu, X.-Z., Zaleski, S., Zanetti, G.: Scaling of hard thermal turbulence in Rayleigh–Bénard convection. J. Fluid Mech. **204**, 1–30 (1989)
10. Chertkov, M., Falkovich, G., Kolokolov, I., Lebedev, V.: Statistics of a passive scalar advected by a large-scale two-dimensional velocity field: analytic solution. Phys. Rev. E **51**, 5609–5627 (1995)
11. Chertkov, M., Kolokolov, G., Vergassola, M.: Inverse cascade and intermittency of passive scalar in one-dimensional smooth flow. Phys. Rev. E **56**, 5483–5499 (1997)
12. Chertkov, M., Falkovich, G., Kolokolov, I.: Intermittent dissipation of a scalar in turbulence. Phys. Rev. Lett. **80**, 2121–2124 (1998)
13. Ching, E.S.C.: Probabilities for temperature differences in Rayleigh–Bénard convection. Phys. Rev. A **44**, 3622–3629 (1991)
14. Holzer, M., Siggia, E.D.: Turbulent mixing of a passive scalar. Phys. Fluids **6**, 1820–1837 (1994)
15. Kraichnan, R.H.: Small-scale structure of a scalar field convected by turbulence. Phys. Fluids **11**, 945–953 (1968)
16. Majda, A.J.: The random uniform shear layer: an explicit example of turbulent diffusion with broad tail probability distributions. Phys. Fluids A **5**, 1963–1970 (1993)
17. Majda, A.J.: Explicit inertial range renormalization theory in a model for turbulent diffusion. J. Stat. Phys. **73**(3–4), 515–542 (1993)
18. Majda, A.J., Kramer, P.: Simplified models for turbulent diffusion: Theory, numerical modelling, and physical phenomenon. Phys. Rep. **314**, 237–574 (1999)
19. McLaughlin, R.M., Majda, A.J.: An explicit example with non-Gaussian probability distribution for nontrivial scalar mean and fluctuation. Phys. Fluids **8**, 536–547 (1996)
20. Pierrehumbert, R.T.: Lattice models of advection-diffusion. Chaos **10**, 61–74 (2000)
21. Pumir, A., Shraiman, B.I., Siggia, E.D.: Exponential tails and random advection. Phys. Rev. Lett. **66**(23), 2984–2987 (1991)

22. Rudin, W.: Real and Complex Analysis. McGraw-Hill, New York (1966)
23. Shraiman, B.I., Siggia, E.D.: Lagrangian path integrals and fluctuations in random flow. Phys. Rev. E **49**(23), 2912–2927 (1994)
24. She, Z.S., Orszag, S.A.: Physical model of intermittency in turbulence: Inertial range non-Gaussian statistics. Phys. Rev. Lett. **66**, 1701–1704 (1991)
25. Sinai, Y.G., Yakhot, V.: Limiting probability distributions of a passive scalar in a random velocity field. Phys. Rev. Lett. **63**, 1962–1964 (1989)
26. Sparling, L.C., Bacmeister, J.T.: Scale dependence of trace microstructure: Pdfs, intermittency and the dissipation scale. Geophys. Res. Lett. **28**, 2823–2826 (2001)
27. Thoroddsen, S.T., Van Atta, C.W.: Exponential tails and skewness of density-gradient probability density functions in stably stratified turbulence. J. Fluid Mech. **244**, 547–566 (1992)
28. Vanden-Eijnden, E.: Non-Gaussian invariant measures for the Majda model of decaying turbulent transport. Commun. Pure Appl. Math. **54**(9), 1146–1167 (2001)